Title
Thermal Conductivity of Biocemented Graded Sands

Journal
Journal of Geotechnical and Geoenvironmental Engineering, 147(10)

ISSN
1090-0241

Authors
Xiao, Yang
Tang, Yifan
Ma, Guoliang
et al.

Publication Date
2021-10-01

DOI
10.1061/(asce)gt.1943-5606.0002621

Peer reviewed

Thermal Conductivity of Biocemented Graded Sands

Yang Xiao, M.ASCE[1]; Yifan Tang[2]; Guoliang Ma[3]; John S. McCartney, F.ASCE[4]; and Jian Chu[5]

Abstract: This paper includes an investigation of the thermal conductivity of biocemented soils to better understanding the regimes of heat transmission through soils treated by microbially induced calcium carbonate precipitation (MICP). A series of thermal conductivity tests using the transient plane source method (TPS) were performed on biocemented silica sand specimens with different gradations, void ratios, and MICP treatment cycles. The results showed that MICP treatment greatly improved the thermal conductivity of sand specimens. An increase in uniformity coefficient or a decrease in void ratio of the sand resulted in an increase in the thermal conductivity of MICP-treated specimens for a given MICP treatment cycle. The increment of thermal conductivity of MICP-treated specimens with respect to that of untreated specimens was also affected by gradation, void ratio and content of calcium carbonate. The greatest improvements in thermal conductivity were achieved for sands having an initial degree of saturation between 0.82 and 0.85. An empirical equation was established to predict the thermal conductivity of MICP-treated silica sand with different variables which may be useful in designing energy piles in biocemented sand layers.

----

[1]Yang Xiao, Ph.D., M.ASCE
Professor, School of Civil Engineering, Chongqing University, State Key Laboratory of Coal Mine Disaster Dynamics and Control, Key Laboratory of New Technology for Construction of Cities in Mountain Area, Chongqing University, Chongqing 400045, China. E-mail: hhuxyanson@163.com

[2]Yifan Tang
Master, School of Civil Engineering, Chongqing University, Chongqing, 400045, China. E-mail: CUtangyifan@163.com

[3]Guoliang Ma
Ph.D. Candidate, School of Civil Engineering, Chongqing University, Chongqing, 400045, China. E-mail: magl09@163.com

[4]John S. McCartney, Ph.D., P.E., F.ASCE
Professor and Department Chair, Dept. of Structural Engineering, University of California San Diego, 9500 Gilman Dr., La Jolla, CA 92093-0085, E-mail: mccartney@ucsd.edu

[5]Jian Chu
Professor, School of Civil and Environmental Engineering, Nanyang Technological University, 10 Blk N1, 50 Nanyang Ave, Singapore 639798. E-mail: cjchu@ntu.edu.sg

Introduction

The use of microbially-induced calcium carbonate precipitation (MICP) in geotechnical engineering has been extensively studied and has several advantages as a soil improvement technique, including lower energy requirements and flexible implementation (Whiffin et al. 2007; DeJong et al. 2010; Al Qabany et al. 2012; Cheng et al. 2013; Chu et al. 2013; Montoya and DeJong 2015; Jiang and Soga 2017; Gomez et al. 2018). MICP leads to an improvement in the mechanical, hydraulic, and thermal properties of sand due to precipitation of $CaCO_3$ between sand particles or on the surface of sand particles (van Paassen 2009; Al Qabany et al. 2012; Cheng et al. 2013; Chu et al. 2013; Montoya and DeJong 2015; O'Donnell and Kavazanjian Jr. 2015; Gomez et al. 2017; Jiang et al. 2017; Gomez et al. 2019; Liu et al. 2019; Montoya et al. 2019; Terzis and Laloui 2019; Xiao et al. 2019a; Ma et al. 2021). This technique was extensively studied in soil stabilization for improving shear strength and dilatancy (DeJong et al. 2006; van Paassen et al. 2010; Chou et al. 2011; Lee et al. 2013; Martinez et al. 2013; Montoya and DeJong 2015; O'Donnell and Kavazanjian Jr. 2015; Venda Oliveira et al. 2015; Feng and Montoya 2016), liquefaction risk reduction (Burbank et al. 2013; Montoya et al. 2013; He and Chu 2014; Sasaki and Kuwano 2016; Feng and Montoya 2017; Xiao et al. 2018a; Xiao et al. 2019a), crack repair (El Mountassir et al. 2014; Minto et al. 2016; Tobler et al. 2018; Minto et al. 2019), and permeability control (Chou et al. 2011; Al Qabany and Soga 2013; Chu et al. 2013; Martinez et al. 2013; Jiang and Soga 2017; Jiang et al. 2017; Wu et al. 2019). MICP has also been applied to enhance the performance of soils surrounding pile foundations (Lin et al. 2016; Lin et al. 2018; Xiao et al. 2020), which implies that there may also be opportunities for using MICP to improve the thermal and mechanical properties of soils surrounding energy piles. Energy pile foundations are formed by incorporating closed-loop geothermal heat exchangers into a cast-in-place pile during construction, and can be used to exchange heat with the subsurface and provide structural support to a building (Brandl 2006; Laloui et al. 2006; Stewart and McCartney 2014; Peric et al. 2020; Ravera et al. 2020). The thermal conductivity of the subsurface is a key variable in the design of energy piles (Brandl 2006; Laloui et al. 2006), as increasing thermal conductivity can increase the ease of heat transfer. This provides the motivation for performing a detailed study on the thermal conductivity of MICP-treated sand.

In soils consisting of mineral particles, water and air, the mineral particles possess much higher thermal conductivity than air and water. For example, the thermal conductivity of quartz is approximately 7 W/m/K and is 11 times larger than that of water at 25 ℃(0.6 W/m/K) and 269 times larger than that of air (0.026 W/m/K) (Yun and Santamarina 2008; Martinez et al. 2019). The thermal conductivity of calcite is approximately 5 W/m/K and slightly less than that of quartz (Martinez et al. 2019). The thermal conductivity of soils is affected by several parameters, including the particle mineralogy, particle size, void ratio, degree of saturation, and cementation (Dong et al. 2015). In order to improve the thermal conductivity, it is difficult to directly change the mineralogy, particle size, porosity and degree of saturation of soils beneath the ground. However, injection of cementation solutions into the ground may be an effective approach to reduce the void ratio of soils. MICP injection is easier than cement injection due to the low viscosity of the treatment solutions (DeJong et al. 2010). Therefore, MICP has a great potential to enhance the performance of energy piles in terms of both mechanical performance (Lin et al. 2016; Lin et al. 2018) and heat exchange performance (Martinez et al. 2019). Treatment of sand layers with MICP may also permit the use of simpler construction techniques to install cast-in-place foundations that do not involve a casing or slurry. Limited studies have been performed to understand the impact of MICP on the thermal conductivity of sand (Venuleo et al. 2016; Martinez et al. 2019; Wang et al. 2020). They investigated the combining effect of MICP bonding and degree of saturation on the thermal conductivity of sand specimens and concluded that the MICP treatment can effectively increase the thermal conductivity of sand specimens. However, the influences of gradation and porosity on the thermal conductivity of

MICP-treated sand specimens are not fully understood. It is important to study the effects of these variables as the gradation and porosity could also influence the thermal conductivity (Xiao et al. 2018b) as well as the precipitation of calcium carbonate. Accordingly, the aim of this study is to systematically investigate the effect of MICP on the thermal conductivity of dry silica sand with different gradations and void ratios and to establish an empirical model for predicting thermal conductivity of MICP-treated sands. The effect of water content and degree of saturation are not considered in the current study.

Materials and Test Protocols

Characteristics of Test Materials

Sand particles in each size group were obtained by sieving Fujian silica sand, the specific gravity of which is 2.69. As shown in **Fig. 1(a)** and **Fig. 1(b)**, four target gradations (i.e., the coefficient of uniformity C_u = 2, 2.8, 4.7 and 9.7) were selected to investigate the effect of gradation on the thermal conductivity of MICP-treated sands. These gradations (Xiao et al. 2018b) were predicted according to the following function (Tyler and Wheatcraft 1992):

$$F(d) = \left(d/d_M\right)^{3-\alpha} \quad \textbf{(1)}$$

where F = percentage finer; d = particle diameter; d_M = maximum particle diameter; and α = fractal dimension. The fractal dimension α obtained from the best-fitting curve ranges from 0.4 to 2.21. The scanning electron micrograph (SEM) images of four mixtures with different gradations are presented in **Fig. 1(c)**. The materials contain more fine particles with increasing C_u. The maximum void ratio $e_{\max}$ and minimum void ratio $e_{\min}$ of each gradation are listed in **Table 1**, which were measured according to standards (ASTM 2016a, b). Three different values of void ratio, i.e., 0.5, 0.6 and 0.7, were selected for each gradation to investigate the effect of void ratio on thermal conductivity. Sand particles were washed with deionized water and oven-dried prior to preparing specimens.

Specimen Preparation and MICP Treatment

As shown in **Fig. 2(a)**, specimens were produced in an acrylic mold with an inner diameter of 65 mm and an inner height of 20 mm. Six holes with a diameter of 5 mm were drilled in the bottom of the mold to permit discharge of excess cementing solution. An annular mold with the same inner size as the acrylic mold without a base was used to contain the cementing solutions for gravity injection. A layer of gauze was placed on the inner base of the mold before specimen preparation. The amount of sand used to prepare each specimen was determined by the target void ratio. The sand was mixed with 6% deaired water and divided into two equal parts. Each part was placed in lifts within the acrylic mold and compacted with a rigid rod following the undercompaction method proposed by Ladd (1978). The density of the upper layer was slightly larger (1%) than that of the lower layer, which can weaken the densification of the lower layer due to the upper-layer compaction, as pointed out by Belkhatir et al. (2011). Next, the annular mold was placed on the specimen and a scouring pad was placed on the top of the specimen to protect the specimen from the disturbance during injection of solutions.

In the current study, *Sporosarcina pasteurii* strain was used to hydrolyze urea. The cultivation of the microbes was the same as that in the work of Xiao et al. (2019b). The cementation solution was composed of 0.1 mol/L of $CaCl_2$ and 0.1 mol/L of urea. The surface percolation (Cheng and Cord-Ruwisch 2012) was used to stabilize specimens, as shown in **Fig. 2(b)**. Specifically, a little more than one pore volume (PV) of bacterial suspension was poured into the annular mold and percolated down through the specimens. The suspension was retained in the specimen for 3 hours to allow the bacteria to be attached on the surface of sand particles. The cementation solution was poured into the annular mold and retained for three hours of reaction, which was repeated five times. The injection procedure can be repeated according to the target cementation level, and each injection of cementation solution is considered to be one treatment cycle. After MICP treatment, specimens were flushed with deionized water, and then oven-dried at 65 ℃ for 48 hours. Finally, these specimens were packed with plastic wrap to avoid absorption of water from the ambient air before the thermal conductivity tests.

To better understand the impact of the degree of saturation of the sand specimens at the time of biocementation treatment, an additional series of tests was performed. The percolation method proposed by Cheng et al. (2013) was used to treat sand specimens (e = 0.5) with different degrees of saturation, where the approach for injection of bacteria and cementation solutions is the same as that used in the main testing program described in **Fig. 2**. A vacuum pump with a funnel connected to the mold of the specimen was used to remove the excess liquid after each injection of bacteria and cementation solutions to reach a target degree of saturation. A membrane was used for sealing the connection between the mold and funnel to avoid the leakage of liquid. Different durations of vacuum application were applied to the cementation solution to reach various degrees of saturation for the different sand specimens. For degrees of saturation larger than 0.8, the extraction of liquid from the specimens is not necessary and gravity drainage was sufficient. The degree of saturation is determined by the retained liquid volume to the initial void volume of the parallel specimens following the standard (ASTM 2019). It should be noted that the degree of saturation reported using this approach is an initial value before cementation, as the void volume of the specimens after biotreatment will decrease by an unknown amount with the production of $CaCO_3$ between sand particles. To keep the same amount of cementation solution, the injection count of cementation solution for one treatment is larger for specimens with lower degrees of saturation that were reached by longer durations of vacuum application.

Measurement of Thermal Conductivity

A Hot Disk Thermal Analyzer (Model TPS2500S from HotDisk of Göteborg, Sweden) was used to measure the thermal conductivity of the specimens through a single-sided heat transfer process with an analysis based on the Transient Plane Source Method (TPS). According to the studies by Gustafsson (1991) and Gustavsson et al. (1994), a double spiral sensor was used for measuring thermal parameters which not only served as a heating source to increase the temperature of the specimen but also as a resistance thermometer to record the temperature increase over time. The sensor was sandwiched between the soil specimen and a piece of foam which functioned as a background material with a known thermal conductivity, as shown in **Fig. 2(c)**. Based on the work by Gustafsson (1991), a constant power is supplied to generate heat through the spiral sensor and increase the temperature, thereby the resistance of the spiral sensor expressed as a function of time can be given as

$$\begin{cases} R(t) = R_0\left[1+\alpha_T \overline{\Delta T(\tau)}\right] \\ \tau = \sqrt{\kappa_\tau t}\Big/ r_s \end{cases} \quad \textbf{(2)}$$

where $R(t)$ is the resistance of the spiral sensor; R_0 is the initial state resistance of the spiral sensor, α_T is the temperature coefficient of the resistivity; $\overline{\Delta T(\tau)}$ is the mean temperature increase of the spiral sensor; τ is the dimensionless time; t is the real time obtained from the beginning of the transient heating; κ_τ is the thermal diffusivity of the tested specimen; and r_s is the overall radius of the spiral sensor. According to Gustafsson (1991), the thermal conductivity of the sample can be given as follows,

$$\lambda = \left[\pi^{-1.5} P_{const} r_s^{-1} \left(\overline{\Delta T(\tau)}\right)^{-1}\right]\left[1\Big/\left(n^2+n\right)^2\right] \int_0^\tau \sum_{i=1}^{n}\sum_{j=1}^{n} \frac{ij}{s^2} \exp\left(-\frac{i^2+j^2}{4n^2 s^2}\right) I_B\left(\frac{ij}{2n^2 s^2}\right) \mathrm{d}s \quad \textbf{(3)}$$

where λ is the thermal conductivity of the tested specimen; P_{const} is the value of the constant power; n is the number of spirals in the sensor; i, j and s are parameters for integral; I_B is a modified

Bessel function (Bohac et al. 2000). The thermal conductivity in **Eq. (3)** is obtained through a process of iteration (Gustafsson 1991; Bohac et al. 2000).

A double spiral sensor with a diameter of 29.2 mm (No. 4922) in **Fig. 2(c)** was selected for use in this study due to its measurement range and accuracy matching the measured values of the thermal conductivity of MICP-treated specimens (Venuleo et al. 2016; Martinez et al. 2019; Wang et al. 2019; Wang et al. 2020). The size of the tested specimen depends on the radius of the selected sensor. According to the manual of the analyzer (Hot Disk Inc 1999), the thickness and diameter of the specimen should be larger than the radius of the sensor (i.e., 14.6 mm). Therefore, a specimen with a radius of 65mm and a thickness of 20mm was sufficient in size and selected for this study. The specimen size is identical to that of the foam specimen that was used as a background material for calibration of the thermal analyzer, as shown in **Fig. 2(c)**. Specimens during tests were placed into the thermal analyzer container that maintained a constant temperature of 25 ℃ to avoid environmental disturbance, as reported in Zhen et al. (2019). In addition, the room temperature of 25 ℃ was controlled by an air conditioner. Triplicate specimens were prepared for each condition, and three thermal conductivity tests were performed on each specimen. The thermal analyzer manual (Hot Disk Inc 1999) stipulates that the measured value of thermal conductivity for a given condition is stable when the deviation of the measured value of these tests to their average value for a given condition does not exceed 2%.The average of the measured values for a given condition was regarded as the representative thermal conductivity of the tested specimen, which are summarized in **Table 2** for both treated and untreated conditions.

Measurement of Calcium Carbonate Content

The acid digestion method was used to determine $CaCO_3$ contents according to the studies of Mortensen et al. (2011), Al Qabany et al. (2012), and Feng and Montoya (2016). Subsamples were taken after thermal conductivity tests, and dried and weighed to obtain the dry mass before HCl dissolution. Then, these subsamples were dissolved by the excess 1M HCl solution for 12 hours until no bubbles were observed. Finally, these subsamples were flushed with deionized water, dried and weighed to obtain the mass of sand after HCl dissolution. The difference between the two measured masses before and after HCl dissolution was taken as the mass of $CaCO_3$, and the $CaCO_3$ content is defined as the ratio of the mass of $CaCO_3$ to the mass of sand:

$$C_{ca} = \left(m_{sca} - m_s\right)/m_s \tag{4}$$

where m_{sca} is the mass of oven-dried MICP-treated sample before HCl dissolution; m_s is the mass of oven-dried MICP-treated sample after HCl dissolution; and C_{ca} is the $CaCO_3$ content.

In the current work, the average $CaCO_3$ content of triplicate specimens at the same condition are regarded as the representative $CaCO_3$ content of the specimen at that condition. The test results show that three measured $CaCO_3$ contents at the same condition are approximately the same, and their deviation to their average value is less than 3.2%.

Thermal Conductivity Results

Thermal Conductivity of Untreated Specimens

Fig. 3(a) shows the thermal conductivity of the untreated specimens. Thermal conductivity of sand specimens at a given void ratio increases at a gradually decreasing rate as C_u increases. Meanwhile, the thermal conductivity of sand specimens at a given gradation decreases linearly with increasing void ratio. This findings for silica sand are consistent with those reported for carbonate sand (Xiao et al. 2018b). Similar to the derivation of empirical equation for thermal conductivity of carbonate sand with respect to the void ratio e and C_u (Xiao et al. 2018b), the following equation for the untreated silica sand is given as

$$\lambda_0 = \lambda_{r0} - k_e^{\lambda} e - k_{cu}^{\lambda} \exp\left(-\chi_{\lambda} C_u\right) \tag{5}$$

where λ_0 denotes the thermal conductivity of the untreated sand specimens; and λ_{r0}, k_e^{λ}, k_{cu}^{λ} and

χ_λ are fitting parameters. The values of these fitting parameters listed in **Table 3** were determined using the statistical method of nonlinear least squares. The fitting surface in **Fig. 3(b)** can reasonably capture the variation of the thermal conductivity of the untreated sand.

Thermal Conductivity of MICP-Treated Specimens

Variations of the thermal conductivity λ of MICP-treated specimens are shown in **Fig. 4**. **Fig. 4(a)** presents the relationship between λ and C_u for different treatment cycles at a given void ratio. For a given treatment cycle N, an increase in C_u leads to an increase in λ. Meanwhile, the rate for the increase of λ at a low value of C_u is much larger when the treatment cycle is 15, which is more obvious at e=0.5. The denser specimen at a given C_u possesses a higher thermal conductivity when the specimen was improved with the same treatment cycle. For a given C_u and e, an increase in the treatment cycle results in a great increase in λ, indicating that MICP treatment could effectively enhance the thermal conductivity of sand, which was also found by Martinez et al. (2019) and Wang et al. (2020). The enhancement was attributed to the increase in contact area and contact points improved by the precipitation of $CaCO_3$ around particle contacts (Yun and Santamarina 2008).

To further explore the influence of $CaCO_3$ precipitation on the thermal conductivity of sand, a thermal conductivity ratio λ_r denoting the increasing times and a thermal conductivity increment $\Delta\lambda$ are proposed and their definitions are given as

$$\lambda_r = \lambda / \lambda_0 \tag{6a}$$

$$\Delta\lambda = \lambda - \lambda_0 \tag{6b}$$

All data on λ_r and $\Delta\lambda$ are listed in **Table 4**.

Fig. 4 (b) and **Fig. 4 (c)** show that an increase in C_u at a given e and N, or an increase in N at a given e and C_u leads to an increase in λ_r and $\Delta\lambda$. In addition, the values of λ_r and

$\Delta\lambda$ at a given C_u and N are larger for specimen at a denser state (i.e., smaller void ratio), indicating that the improvement of MICP on the thermal conductivity is also more effective for a denser sand. For C_u = 9.7, e = 0.5 and N = 15, the thermal conductivity ratio λ_r is 3.04, denotating that the thermal conductivity (1.61 W/m/K) of the MICP-treated sand is 3 times larger than that of the untreated sand (0.53 W/m/K). The maximum thermal conductivity ratio reported in the literature was 4.3 in Martinez et al. (2019) and 2.3 in Wang et al. (2020), implying that the MICP treatment can effectively improve the thermal conductivity of sands, which is meaningful to enhance the performance of the soil surrounding energy piles.

$CaCO_3$ Contents of MICP-Treated Specimens

The $CaCO_3$ content, a significant factor for improving the engineering properties of soil (Chu et al. 2013; Gomez et al. 2017; Gomez et al. 2019; Montoya et al. 2019), can be influenced in turn by soil matrix characteristics, e.g., saturation (Cheng et al. 2013), particle size (Nafisi et al. 2020) and particle shape (Xiao et al. 2019d). **Fig. 5** shows the $CaCO_3$ content of MICP-treated specimens with different values of C_u, e and N. Comparisons of **Figs. 5(a-c)** obviously show that an increase in the treatment cycle leads to an increase in $CaCO_3$ content. For a given treatment cycle, the $CaCO_3$ content increases with decreasing e at a given C_u or with increasing C_u at a given e. For example, the $CaCO_3$ content of MICP-treated specimen with e = 0.5 increases from 0.82% to 1.22% for N = 5, from 1.8% to 2.21% for N = 10, and from 2.81% to 3.52% for N = 15, as C_u increases from 2 to 9.7.

For a partially saturated condition, the air is assumed to occupy the center of the pores with a water film covering the surface of the grains, forming menisci (Lu and Likos 2004; Lu and Dong 2015; Lu and Zhang 2019; Lu 2020). A surface percolation method for MICP treatment under unsaturated conditions proposed by Cheng and Cord-Ruwisch (2012) was adopted in the current study.

The distribution of the bacterial and cementation solutions of specimens in this method ranges from the pendular to capillary regimes of the pore-water distribution (Dong et al. 2015). $CaCO_3$ crystals formed in the solutions distribute at the same location of the solutions: particle contacts surrounded by liquid menisci and particle surface. $CaCO_3$ crystals located at particle contacts are more effective than that at particle surface in improvement of strength, as observed by Cheng et al. (2013). The amount of $CaCO_3$ crystals is determined by the water retention properties of sand, i.e., the retention of bacterial and cementation solutions. Soils with smaller pores will retain more water at higher suctions (Lu and Likos 2004). The sand specimen with a large value of C_u which contains more fine particles would retain more cementation and bacterial solutions for biochemical reaction and thereby result in more precipitation of $CaCO_3$ around sand grains. This conforms with the above observations that the $CaCO_3$ content of oven-dried MICP-treated specimens at the same condition increases with increasing C_u.

Predictions of Thermal Conductivity

Figs. 6(a-d) show the relationship between the thermal conductivity increment $\Delta\lambda$ and the $CaCO_3$ content C_{ca} of MICP-treated specimens with C_u = 2, 2.7, 4.7 and 9.7, respectively. The basic trend for this relationship with different values of C_u is similar, which can be described by the following equation:

$$\Delta\lambda = \beta\left(C_{ca}\right)^{\vartheta} \quad \textbf{(7)}$$

where β and ϑ are empirical fitting parameters. Their values listed in **Table 5** at different coefficients of uniformity and void ratios were determined using the statistical method of nonlinear least squares. As shown in **Figs. 6(a-d)**, the tangent slope of the fitting curves for the relationship between $\Delta\lambda$ and C_{ca} at a given C_{ca} increases with an increase in C_u for MICP-treated specimens with the same void ratio. **Fig. 7(a)** shows that the parameter β at a given C_u decreases almost linearly with increasing void ratio, meanwhile the parameter β at a given void ratio increases exponentially with increasing C_u. Therefore, the parameter β with respect to C_u and e can be described by the following equation:

$$\beta=\left(\beta_0-k_e^{\beta}e\right)\left[1-\left(C_u\right)^{-\chi_\beta}\right] \tag{8}$$

where β_0, k_e^{β} and χ_β are fitting parameters. **Fig. 7(b)** shows that the predictions by **Eq. (8)** are in good agreement with the data of β. As shown in **Fig. 7(c)**, the relationship between the parameter ϑ and C_u can be described by an exponential function:

$$\vartheta=\vartheta_0-k_{cu}^{\vartheta}\exp\left(-\chi_\vartheta C_u\right) \tag{9}$$

where ϑ_0, k_{cu}^{ϑ} and χ_ϑ are fitting parameters. The values of fitting parameters in **Table 3** (β_0, k_e^{β}, χ_β, ϑ_0, k_{cu}^{ϑ} and χ_ϑ) were also determined using the statistical method of nonlinear least squares. Substitution of **Eqs. (8)** and **(9)** into **Eq. (7)** gives

$$\Delta\lambda=\left(\beta_0-k_e^{\beta}e\right)\left[1-\left(C_u\right)^{-\chi_\beta}\right]\left(C_{ca}\right)^{\vartheta_0-k_{cu}^{\vartheta}\exp\left(-\chi_\vartheta C_u\right)} \tag{10}$$

As shown in **Fig. 8**, **Eq. (10)** with the calibrated parameters can well predict the increment of thermal conductivity of MICP-treated specimens at different $CaCO_3$ contents, coefficients of uniformity and void ratios with $R^2\geq 0.92$. The predictions of the thermal conductivity for MICP-treated specimens can be obtained by combining **Eqs. (5)** and **(10)**:

$$\begin{aligned}\lambda=\lambda_0+\Delta\lambda=\lambda_{r0}-k_e^{\lambda}e-k_{cu}^{\lambda}\exp\left(-\chi_\lambda C_u\right)+\\ \left(\beta_0-k_e^{\beta}e\right)\left[1-\left(C_u\right)^{-\chi_\beta}\right]\left(C_{ca}\right)^{\vartheta_0-k_{cu}^{\vartheta}\exp\left(-\chi_\vartheta C_u\right)}\end{aligned} \tag{11}$$

Fig. 9 shows the comparisons between the predictions by **Eq. (11)** and test data on the thermal conductivity for MICP-treated specimens at different $CaCO_3$ contents, coefficients of uniformity, and void ratios. Obviously, the empirical **Eq. (11)** with the calibrated parameters can well capture the variations of the thermal conductivity of MICP-treated specimens with the $CaCO_3$ content, coefficient of uniformity, and void ratio.

There are many factors affecting the thermal conductivity of sand, including properties of the sand and environment conditions (Dong et al. 2015; Zhang and Wang 2017). However, this study focuses on the effects of cementation, gradation, and void ratio on the thermal conductivity of dry sand. Therefore, the proposed empirical model does not incorporate the influence of mineral composition, particle shape, particle size, water content, degree of saturation, temperature, etc. As the empirical model in the current study is proposed for dry specimens, it cannot be used to predict the test data with different water contents from Venuleo et al. (2016). Another difference between the current work and the work by Wang et al. (2020) is that the base sands possess different mineral compositions. In the current work, the sand is composed of 99.5% quartz, while the sand in the work by Wang et al. (2020) only contains 56% quartz. As pointed out by Dong et al. (2015), the mineral composition plays a key role in the thermal conductivity of soils. The thermal conductivity is higher for sand with a higher quartz content. Furthermore, the MICP treatment strategy could affect the location of precipitates and crystal size (Cheng et al. 2013). For example, $CaCO_3$ is more likely to precipitate around particle contacts when the specimens are treated at an unsaturated condition as conducted in the current work and other studies (Cheng and Cord-Ruwisch 2012; Cheng et al. 2013), while more $CaCO_3$ would precipitate on the sand surface in saturated conditions as conducted in the work by Wang et al. (2020). The $CaCO_3$ precipitated around the particle contacts would contribute more to thermal conductivity while the $CaCO_3$ precipitated on the surface of sand would contribute less to the thermal conductivity. Therefore, the test data from Wang et al. (2020) could not be predicted by the proposed equation. The effect of location of $CaCO_3$ on thermal conductivity can be analogized to the effect of the degree of saturation on thermal conductivity proposed by Dong et al. (2015).

Predictions of $\Delta\lambda$ and λ shown in **Figs. 10(a)** and **10(b)** are in good agreement with all the test data from the current study. As the mineral composition of sand in this study is the same as that in Martinez et al. (2019), the proposed empirical model, i.e., **Eq. (11)**, was also used to predict the test data on $\Delta\lambda$ and λ of dry sand specimens reported by Martinez et al. (2019). A shown in **Figs. 10(c)** - **10(f)**, the proposed model with other values of parameters β_0, ϑ_0 and χ_ϑ can well predict the test data on $\Delta\lambda$ and λ ($R^2 \geq 0.92$) but slightly overestimate the values of λ at the low $CaCO_3$ content. The different values of β_0, ϑ_0 and χ_ϑ between the sand in the current study and the sand in the study of Martinez et al. (2019) is mainly attributed to different MICP treatment strategies and different particle sizes of the sand for a given C_u. Previous studies found that the particle size could greatly influence the thermal conductivity of sands (Lee et al. 2015; Xiao et al. 2019c; Zhang et al. 2019; Zhang et al. 2020).

Effect of Saturation on $CaCO_3$ Content and Thermal Conductivity

As the surface percolation method of MICP treatment is performed under unsaturated conditions, it is useful to explore the effects of initial degree of saturation on the $CaCO_3$ content and thermal conductivity of biocemented sands. The results in **Fig. 11(a)** show that the $CaCO_3$ content for specimens with C_u = 2 increases with increasing degree of saturation (S_r) to a peak value (C_{ca} = 1.8%) at S_r = 0.82 then decreases sharply until reaching saturation S_r = 1. Consistent with the previous results, greater $CaCO_3$ contents are observed for sands with greater coefficients of uniformity of the sand, but an interesting observation is that the coefficient of uniformity plays a major role in the trends in $CaCO_3$ content with degree of saturation. Below the peak, greater increases in $CaCO_3$ content are observed for sands with lower coefficients of uniformity. The decreases in $CaCO_3$ content with increasing degrees of saturation beyond the peak are similar for all the sand specimens with different coefficients of uniformity. The effect of initial degree of saturation on the thermal conductivity shown in **Fig. 11(b)** is similar to the effect of degree of saturation on $CaCO_3$ content in **Fig. 11(a)**. The thermal conductivity increases with degree of saturation to a peak value then decreases sharply until approaching saturated conditions. The minimum value of the $CaCO_3$ content and thermal conductivity is observed for S_r =1 for all coefficients of uniformity in the tested degrees of saturation (S_r greater than 0.4). The results in Fig. 11(b) confirm that the use of fully saturated conditions during MICP is not an effective strategy to improve the thermal conductivity of sand. It is noted that it is difficult to perform MICP treatment on sands with very low degrees of saturation (S_r smaller than 0.4), especially for specimens with large coefficient of uniformity, as the excessive extraction of liquid from specimens would result in a nonuniform $CaCO_3$ distribution across the specimen. The optimal degree of saturation for MICP treatment to improve the thermal conductivity ranges from 0.82 to 0.85 and increases slightly with increasing coefficient of uniformity. Predictions of the thermal conductivity for sands having different degrees of saturations are shown in **Fig. 11(c)** as triangular points, which are in agreement with other conditions investigated in this study. In general, all data points fall into a narrow band around the 1:1 fitting line indicating a satisfactory prediction.

Microanalysis of Thermal Conductivity of MICP-Treated Sand

In the current study, the distributions of $CaCO_3$ on particle surface and around particle contacts were observed. However, $CaCO_3$ formation around particle contacts rather than on particle surfaces can effectively increase the contact area, coordination number, and thereby the thermal conductivity of sand assembles (Yun and Santamarina 2008; Tarnawski and Leong 2016). To better understand the $CaCO_3$ formation process on a microscale, scanning electron microscope (SEM) images were obtained for treated and untreated sands. SEM images are shown in **Figs. 12(a-f)** for MICP-treated specimens with the same void ratio (e = 0.5) but different gradation (C_u = 2 (a and b) and C_u =

9.7 (c and d)) under the same treatment cycle (N = 15). $CaCO_3$ crystals are observed on the surface of sand particles when C_u = 2, as shown in **Figs. 12(a-c)**, leading to non-contacts shown in **Fig. 12(c)**. However, comparison of the images in **Fig.12(a)** with **12(d)** indicate that the contact points of MICP-treated specimens with C_u = 2 are greater than in specimens with C_u = 9.7. In addition, it is difficult to differentiate the $CaCO_3$ crystals and fine particles when C_u = 9.7, as shown in **Fig. 12(e-f)**. The $CaCO_3$ crystals in **Fig. 12(e)** tend to mix with fine sand and fill the pores between coarse sand particles, resulting in the enhancement in the coordination number and contact area with a large coefficient of uniformity, as shown in **Fig. 12(f)**. Mahawish et al. (2018) also observed from their tests that adding fine aggregate to coarse sand matrix could provide more bridging contacts between coarse sand particles during the MICP process. As a result, more thermal bridges were formed between sand particles at C_u = 9.7 after MICP treatment, which conforms that the thermal conductivity of MICP-treated specimen at a given void ratio and treatment cycle increases as the coefficient of uniformity increases. SEM images in **Figs. 13(a-d)** show MICP-treated specimens with the same gradation (C_u = 2.8) but different void ratios (e = 0.5 (a and b) and e = 0.7 (c and d)) under the same treatment cycle (N = 15). More $CaCO_3$ crystals grow in the dense sand compared with that in the loose sand (**Fig. 13 (a and c)**), which is consistent with the results of $CaCO_3$ contents. This observation may be contributed to that the dense sand would retain more solutions than the loose sand, as reported by Zhou et al. (2014). More solutions in the dense sand can result in more crystal precipitation at particle contacts to form “thermal bridges”, as compared **Fig 13(b)** with **(d)**, leading to a higher thermal conductivity increment in denser specimens than in looser specimens.

Conclusions

A series of thermal conductivity tests were carried out to investigate the effect of MICP treatment, gradation and density on the thermal conductivity of MICP-treated sand. The main conclusions are summarized as follows:

(1) Thermal conductivity of untreated sand specimens and MICP-treated sand specimens at a given treatment cycle increased with increasing coefficient of uniformity at a given void ratio or with decreasing void ratio at a given coefficient of uniformity. In addition, for a given treatment cycle, an increase in coefficient of uniformity or a decrease in void ratio resulted in an increase in the increment of thermal conductivity and the $CaCO_3$ content of MICP-treated specimens.

(2) MICP treatment can greatly enhance the thermal conductivity of sand. For example, the thermal conductivity of a MICP-treated sand specimen (1.61 W/m/K) at C_u = 9.7 and e = 0.5 was 3 times larger than that of an untreated sand specimen (0.53 W/m/K) when the treatment cycle was 15. The MICP enhancement in thermal conductive ability of sand at a given treatment cycle was more obviously at a large coefficient of uniformity or at a dense state, which was validated by the SEM images of MICP-treated specimens. It was found that the greatest thermal conductivity values were obtained for sand specimens having initial degrees of saturation between 0.82 and 0.85, and that the impact of degree of saturation on $CaCO_3$ content and thermal conductivity was very sensitive to the coefficient of uniformity.

(3) An empirical equation for the thermal conductivity was established for MICP-treated silica sand that considered the combined effects of biocementation, gradation and void ratio. This empirical equation provided a good fit to the test data of MICP-treated silica sand specimens at different $CaCO_3$ contents, coefficients of uniformity, and void ratios.

The current study demonstrates that MICP treatment is a feasible approach to improve the thermal conductivity of sand, especially for denser sands having higher coefficients of uniformity. The results in this study indicate that there may be opportunities to use MICP to improve the in-situ thermal conductivity of sands to enhance the efficiency of energy piles used in tandem with ground source heat pumps.

Data Availability

All data, models, and code generated or used during the study appear in the submitted article.

Acknowledgments

The authors would like to acknowledge the financial support from the National Nature Science Foundation of China (Grant No. 41831282, Grant No. 51922024 and Grant No. 51678094). We also appreciate the help of Prof. Huyuan Zhang from Lanzhou University in the use of the Thermal Constant Analyzer.

References

Al Qabany, A., and K. Soga (2013). "Effect of chemical treatment used in MICP on engineering properties of cemented soils." *Géotechnique*, 63(4), 331-339.

Al Qabany, A., K. Soga, and C. Santamarina (2012). "Factors Affecting Efficiency of Microbially Induced Calcite Precipitation." *J. Geotech. Geoenviron. Eng.*, 138(8), 992-1001.

ASTM (2016a). "Standard test methods for maximum index density and unit weight of soils using a vibratory table." *D4253-16*, West Conshohocken, PA.

ASTM (2016b). "Standard test methods for minimum index density and unit weight of soils and calculation of relative density." *D4254-16*, West Conshohocken, PA.

ASTM (2019). "Standard Test Methods for Laboratory Determination of Water (Moisture) Content of Soil and Rock by Mass." *D2216*, West Conshohocken, PA.

Belkhatir, M., A. Arab, T. Schanz, H. Missoum, and N. Della (2011). "Laboratory study on the liquefaction resistance of sand-silt mixtures: effect of grading characteristics." *Granul. Matter*, 13(5), 599-609.

Bohac, V., M. K. Gustavsson, L. Kubicar, and S. E. Gustafsson (2000). "Parameter estimations for measurements of thermal transport properties with the hot disk thermal constants analyzer." *Rev.*

Sci. Instrum., 71(6), 2452-2455.

Brandl, H. (2006). "Energy foundations and other thermo-active ground structures." *Geotechnique*, 56(2), 81-122.

Burbank, M., T. Weaver, R. Lewis, T. Williams, B. Williams, and R. Crawford (2013). "Geotechnical Tests of Sands Following Bioinduced Calcite Precipitation Catalyzed by Indigenous Bacteria." *J. Geotech. Geoenviron. Eng.*, 139(6), 928-936.

Cheng, L., and R. Cord-Ruwisch (2012). "In situ soil cementation with ureolytic bacteria by surface percolation." *Ecol. Eng.*, 42(May), 64-72.

Cheng, L., R. Cord-Ruwisch, and M. A. Shahin (2013). "Cementation of sand soil by microbially induced calcite precipitation at various degrees of saturation." *Can. Geotech. J.*, 50(1), 81-90.

Chou, C.-W., E. A. Seagren, A. H. Aydilek, and M. Lai (2011). "Biocalcification of Sand through Ureolysis." *J. Geotech. Geoenviron. Eng.*, 137(12), 1179-1189.

Chu, J., V. Ivanov, M. Naeimi, V. Stabnikov, and B. Li (2013). "Microbial method for construction of an aquaculture pond in sand." *Géotechnique*, 63(10), 871-875.

DeJong, J. T., M. Fritzges, B. , and K. Nüsslein (2006). "Microbially Induced Cementation to Control Sand Response to Undrained Shear." *J. Geotech. Geoenviron. Eng.*, 132(11), 1381-1392.

DeJong, J. T., B. M. Mortensen, B. C. Martinez, and D. C. Nelson (2010). "Bio-mediated soil improvement." *Ecol. Eng.*, 36(2), 197-210.

Dong, Y., J. S. McCartney, and N. Lu (2015). "Critical review of thermal conductivity models for unsaturated Soils." *Geotech. Geol. Eng.*, 33(2), 207-221.

El Mountassir, G., R. J. Lunn, H. Moir, and E. MacLachlan (2014). "Hydrodynamic coupling in microbially mediated fracture mineralization: Formation of self-organized groundwater flow channels." *Water Resour. Res.*, 50(1), 1-16.

Feng, K., and B. M. Montoya (2016). "Influence of Confinement and Cementation Level on the

Behavior of Microbial-Induced Calcite Precipitated Sands under Monotonic Drained Loading." *J. Geotech. Geoenviron. Eng.*, 142(1), 04015057.

Feng, K., and B. M. Montoya (2017). "Quantifying Level of Microbial-Induced Cementation for Cyclically Loaded Sand." *J. Geotech. Geoenviron. Eng.*, 143(6), 06017005.

Gomez, M. G., C. M. Anderson, C. M. R. Graddy, J. T. DeJong, D. C. Nelson, and T. R. Ginn (2017). "Large-Scale Comparison of Bioaugmentation and Biostimulation Approaches for Biocementation of Sands." *J. Geotech. Geoenviron. Eng.*, 143(5), 04016124.

Gomez, M. G., C. M. R. Graddy, J. T. DeJong, and D. C. Nelson (2019). "Biogeochemical Changes During Bio-cementation Mediated by Stimulated and Augmented Ureolytic Microorganisms." *Scientifc Reports*, 9(1), 11517.

Gomez, M. G., C. M. R. Graddy, J. T. DeJong, D. C. Nelson, and M. Tsesarsky (2018). "Stimulation of Native Microorganisms for Biocementation in Samples Recovered from Field-Scale Treatment Depths." *J. Geotech. Geoenviron. Eng.*, 144(1), 04017098.

Gustafsson, S. E. (1991). "Transient plane source techniques for thermal conductivity and thermal diffusivity measurements of solid materials." *Rev. Sci. Instrum.*, 62(3), 797-804.

Gustavsson, M., E. Karawacki, and S. E. Gustafsson (1994). "Thermal conductivity, thermal diffusivity, and specific heat of thin samples from transient measurements with hot disk sensors." *Rev. Sci. Instrum.*, 65(12), 3856-3859.

He, J., and J. Chu (2014). "Undrained Responses of Microbially Desaturated Sand under Monotonic Loading." *J. Geotech. Geoenviron. Eng.*, 140(5), 04014003.

Hot Disk Inc (1999). *Hot Disk Thermal Constants Analyzer*, Uppsala, Sweden: Hot Disk.

Jiang, N.-J., and K. Soga (2017). "The applicability of microbially induced calcite precipitation (MICP) for internal erosion control in gravel–sand mixtures." *Géotechnique*, 67(1), 42-55.

Jiang, N.-J., K. Soga, and M. Kuo (2017). "Microbially Induced Carbonate Precipitation for Seepage-

Induced Internal Erosion Control in Sand-Clay Mixtures." *J. Geotech. Geoenviron. Eng.*, 143(3), 04016100

Ladd, R. S. (1978). "Preparing test specimens using undercompaction." *Geotech. Test. J.*, 1(1), 16-23.

Laloui, L., M. Nuth, and L. Vulliet (2006). "Experimental and numerical investigations of the behaviour of a heat exchanger pile." *Int. J. Numer. Anal. Met.*, 30(8), 763-781.

Lee, J., T. S. Yun, and S. U. Choi (2015). "The effect of particle sze on thermal conduction in granular mixtures." *Materials*, 8(7), 3975-3991.

Lee, M. L., W. S. Ng, and Y. Tanaka (2013). "Stress-deformation and compressibility responses of bio-mediated residual soils." *Ecol. Eng.*, 60(Nov), 142-149.

Lin, H., M. T. Suleiman, H. M. Jabbour, and D. G. Brown (2018). "Bio-grouting to enhance axial pull-out response of pervious concrete ground improvement piles." *Can. Geotech. J.*, 55(1), 119-130.

Lin, H., M. T. Suleiman, H. M. Jabbour, D. G. Brown, and E. Kavazanjian Jr. (2016). "Enhancing the Axial Compression Response of Pervious Concrete Ground Improvement Piles Using Biogrouting." *J. Geotech. Geoenviron. Eng.*, 142(10), 04016045.

Liu, L., H. Liu, A. W. Stuedlein, T. M. Evans, and Y. Xiao (2019). "Strength, Stiffness, and Microstructure Characteristics of Biocemented Calcareous Sand." *Can. Geotech. J.*, 56(10), 1502-1513.

Lu, N. (2020). "Unsaturated Soil Mechanics: Fundamental Challenges, Breakthroughs, and Opportunities." *J. Geotech. Geoenviron. Eng.*, 146(5), 02520001.

Lu, N., and Y. Dong (2015). "Closed-Form Equation for Thermal Conductivity of Unsaturated Soils at Room Temperature." *J. Geotech. Geoenviron. Eng.*, 141(6), 04015016.

Lu, N., and W. J. Likos (2004). *Unsaturated Soil Mechanics*, John Wiley & Sons, Hoboken, NJ.

Lu, N., and C. Zhang (2019). "Soil Sorptive Potential: Concept, Theory, and Verification." *J. Geotech. Geoenviron. Eng.*, 145(4), 04019006.

Ma, G., X. He, X. Jiang, H. Liu, J. Chu, and Y. Xiao (2021). "Strength and Permeability of Bentonite-Assisted Biocemented Coarse Sand." *Can. Geotech. J.*, 57, https://doi.org/10.1139/cgj-2020-0045.

Mahawish, A., A. Bouazza, and W. P. Gates (2018). "Effect of particle size distribution on the bio-cementation of coarse aggregates." *Acta Geotechnica*, 13(4), 1019-1025.

Martinez, A., L. Huang, and M. G. Gomez (2019). "Thermal conductivity of MICP-treated sands at varying degrees of saturation." *Geotech. Lett.*, 9(1), 15-21.

Martinez, B. C., J. T. DeJong, T. R. Ginn, B. M. Montoya, T. H. Barkouki, C. Hunt, B. Tanyu, and D. Major (2013). "Experimental optimization of microbial-induced carbonate precipitation for soil improvement." *J. Geotech. Geoenviron. Eng.*, 139(4), 587-598.

Minto, J. M., R. J. Lunn, and G. El Mountassir (2019). "Development of a Reactive Transport Model for Field-Scale Simulation of Microbially Induced Carbonate Precipitation." *Water Resour. Res.*, 55(8), 7229-7245.

Minto, J. M., E. MacLachlan, G. El Mountassir, and R. J. Lunn (2016). "Rock fracture grouting with microbially induced carbonate precipitation." *Water Resour. Res.*, 52(11), 8810-8827.

Montoya, B. M., and J. T. DeJong (2015). "Stress-strain behavior of sands cemented by microbially induced calcite precipitation." *J. Geotech. Geoenviron. Eng.*, 141(6), 04015019.

Montoya, B. M., J. T. DeJong, and R. W. Boulanger (2013). "Dynamic response of liquefiable sand improved by microbial-induced calcite precipitation." *Géotechnique*, 63(4), 302-312.

Montoya, B. M., S. Safavizadeh, and M. A. Gabr (2019). "Enhancement of Coal Ash Compressibility Parameters Using Microbial-Induced Carbonate Precipitation." *J. Geotech. Geoenviron. Eng.*, 145(5), 04019018.

Mortensen, B. M., M. J. Haber, J. T. DeJong, L. F. Caslake, and D. C. Nelson (2011). "Effects of environmental factors on microbial induced calcium carbonate precipitation." *J. Appl. Microbiol.*, 111(2), 338-349.

Nafisi, A., B. M. Montoya, and T. M. Evans (2020). "Shear Strength Envelopes of Biocemented Sands with Varying Particle Size and Cementation Level." *J. Geotech. Geoenviron. Eng.*, 146(3), 04020002.

O'Donnell, T. S., and E. Kavazanjian Jr. (2015). "Stiffness and Dilatancy Improvements in Uncemented Sands Treated through MICP." *J. Geotech. Geoenviron. Eng.*, 141(11), 02815004.

Peric, D., A. E. Cossel, and S. A. Sarna (2020). "Analytical Solutions for Thermomechanical Soil Structure Interaction in End-Bearing Energy Piles." *J. Geotech. Geoenviron. Eng.*, 146(7), 04020047.

Ravera, E., M. Sutman, and L. Laloui (2020). "Load Transfer Method for Energy Piles in a Group with Pile-Soil-Slab-Pile Interaction." *J. Geotech. Geoenviron. Eng.*, 146(6), 04020042.

Sasaki, T., and R. Kuwano (2016). "Undrained cyclic triaxial testing on sand with non-plastic fines content cemented with microbially induced CaCO3." *Soils Found.*, 56(3), 485-495.

Stewart, M. A., and J. S. McCartney (2014). "Centrifuge Modeling of Soil-Structure Interaction in Energy Foundations." *J. Geotech. Geoenviron. Eng.*, 140(4), 04013044.

Tarnawski, V. R., and W. H. Leong (2016). "Advanced geometric mean model for predicting thermal conductivity of unsaturated soils." *Int. J. Thermophys.*, 37(2), 18.

Terzis, D., and L. Laloui (2019). "Cell-free soil bio-cementation with strength, dilatancy and fabric characterization." *Acta Geotechnica*, 14(3), 639-656.

Tobler, D. J., J. M. Minto, G. El Mountassir, R. J. Lunn, and V. R. Phoenix (2018). "Microscale Analysis of Fractured Rock Sealed With Microbially Induced CaCO3 Precipitation: Influence on Hydraulic and Mechanical Performance." *Water Resour. Res.*, 54(10), 8295-8308.

Tyler, S. W., and S. W. Wheatcraft (1992). "Fractal Scaling of Soil Particle-Size Distributions: Analysis and Limitations." *Soil Sci. Soc. Am. J.*, 56(2), 362-369.

van Paassen, L. A. (2009). "Biogrout, ground improvement by microbial induced carbonate precipitation." Ph.D. Thesis, Delft University of Technology, Delft.

van Paassen, L. A., R. Ghose, T. J. M. van der Linden, W. R. L. van der Star, and M. C. M. van Loosdrecht (2010). "Quantifying biomediated ground improvement by ureolysis: Large-scale biogrout experiment." *J. Geotech. Geoenviron. Eng.*, 136(12), 1721-1728.

Venda Oliveira, P. J., M. S. da Costa, J. N. P. Costa, and M. Fernanda Nobre (2015). "Comparison of the Ability of Two Bacteria to Improve the Behavior of Sandy Soil." *J. Mater. Civil. Eng.*, 27(1), 06014025.

Venuleo, S., L. Laloui, D. Terzis, T. Hueckel, and M. Hassan (2016). "Microbially induced calcite precipitation effect on soil thermal conductivity." *Geotech. Lett.*, 6(1), 39-44.

Wang, Z., N. Zhang, J. Ding, Q. Li, and J. Xu (2020). "Thermal conductivity of sands treated with microbially induced calcite precipitation (MICP) and model prediction." *Int. J. Heat Mass. Tran*, 147(Feb), 118899.

Wang, Z., N. Zhang, F. Lin, J. Ding, and H. Yang (2019). "Thermal Conductivity of Dry Sands Treated with Microbial-Induced Calcium Carbonate Precipitation." *Advances in Materials Science and Engineering*, 2019(Feb), 4562958.

Whiffin, V. S., L. A. van Paassen, and M. P. Harkes (2007). "Microbial Carbonate Precipitation as a Soil Improvement Technique." *Geomicrobiol. J.*, 24(5), 417-423.

Wu, C., J. Chu, S. Wu, and W. Guo (2019). "Quantifying the Permeability Reduction of Biogrouted Rock Fracture." *Rock. Mech. Rock. Eng.*, 52(3), 947-954.

Xiao, P., H. Liu, A. W. Stuedlein, T. M. Evans, and Y. Xiao (2019a). "Effect of Relative Density and Bio-cementation on the Cyclic Response of Calcareous Sand." *Can. Geotech. J.*, 56(12), 1849-

1862.

Xiao, P., H. Liu, Y. Xiao, A. W. Stuedlein, and T. M. Evans (2018a). "Liquefaction resistance of bio-cemented calcareous sand." *Soil Dyn. Earthq. Eng.*, 107, 9-19.

Xiao, Y., X. He, T. M. Evans, A. W. Stuedlein, and H. Liu (2019b). "Unconfined Compressive and Splitting Tensile Strength of Basalt Fiber-Reinforced Biocemented Sand." *J. Geotech. Geoenviron. Eng.*, 145(9), 04019048.

Xiao, Y., H. L. Liu, B. Nan, and J. S. McCartney (2018b). "Gradation-dependent thermal conductivity of sands." *J. Geotech. Geoenviron. Eng.*, 144(9), 06018010.

Xiao, Y., B. Nan, and J. S. McCartney (2019c). "Thermal Conductivity of Sand-Tire Shred Mixtures." *J. Geotech. Geoenviron. Eng.*, 145(11), 06019012.

Xiao, Y., A. W. Stuedlein, Z. Pan, H. Liu, T. M. Evans, X. He, H. Lin, J. Chu, and L. A. van Paassen (2020). "Toe Bearing Capacity of Precast Concrete Piles through Biogrouting Improvement." *J. Geotech. Geoenviron. Eng.*, 146(12), 06020026.

Xiao, Y., A. W. Stuedlein, J. Ran, T. M. Evans, L. Cheng, H. Liu, L. A. van Paassen, and J. Chu (2019d). "Effect of Particle Shape on Strength and Stiffness of Biocemented Glass Beads." *J. Geotech. Geoenviron. Eng.*, 145(11), 06019016.

Yun, T. S., and J. C. Santamarina (2008). "Fundamental study of thermal conduction in dry soils." *Granul. Matter*, 10(Mar), 197-207.

Zhang, N., and Z. Wang (2017). "Review of soil thermal conductivity and predictive models." *Int. J. Therm. Sci.*, 117(Jul), 172-183.

Zhang, N., X. Yu, A. Pradhan, and A. J. Puppala (2019). "Effects of Particle Size and Fines Content on Thermal Conductivity of Quartz Sands." *Transport. Res. Rec.*, 2510(1), 36-43.

Zhang, X. R., G. Q. Kong, L. H. Wang, and X. L. Xu (2020). "Measurement and prediction on thermal conductivity of fused quartz." *Scientifc Reports*, 10(1), 6559.

Zhen, Z.-l., G.-l. Ma, H.-y. Zhang, Y.-x. Gai, and Z.-y. Su (2019). "Thermal Conductivities of Remolded and Undisturbed Loess." *J. Mater. Civil. Eng.*, 31(2), 04018379.

Zhou, W.-H., K.-V. Yuen, and F. Tan (2014). "Estimation of soil-water characteristic curve and relative permeability for granular soils with different initial dry densities." *Eng. Geol.*, 179(Sep), 1-9.

Table 1. Maximum and minimum void ratios of sand samples with different gradations

Gradation	C_u	α	$e_{\min}$	$e_{\max}$
G1	2	0.40	0.48	0.82
G2	2.8	1.25	0.42	0.8
G3	4.7	1.85	0.37	0.78
G4	9.7	2.21	0.3	0.74

Note: C_u = coefficient of uniformity; α = fractal dimension; $e_{\min}$ = minimum void ratio; and $e_{\max}$ = maximum void ratio

Table 2. Test results on thermal conductivity of untreated and biocemented sands

e	N	C_u	λ (W/m/K)
0.5	0	2	0.46
		2.8	0.48
		4.7	0.51
		9.7	0.53
	5	2	0.69
		2.8	0.80
		4.7	0.95
		9.7	1.00
	10	2	0.83
		2.8	1.03
		4.7	1.19
		9.7	1.28
	15	2	0.96
		2.8	1.23
		4.7	1.45
		9.7	1.61
0.6	0	2	0.43
		2.8	0.45
		4.7	0.48
		9.7	0.51
	5	2	0.62
		2.8	0.73
		4.7	0.80
		9.7	0.87
	10	2	0.74
		2.8	0.89
		4.7	1.01
		9.7	1.08
	15	2	0.85
		2.8	1.07
		4.7	1.22
		9.7	1.34
0.7	0	2	0.40
		2.8	0.42
		4.7	0.44
		9.7	0.47
	5	2	0.57
		2.8	0.62
		4.7	0.70

		9.7	0.76
	10	2	0.64
		2.8	0.75
		4.7	0.84
		9.7	0.90
	15	2	0.73
		2.8	0.89
		4.7	1.02
		9.7	1.08

Note: e = void ratio; N = treatment cycles; and λ = thermal conductivity (Unit: W/m/K).

Table 3. Fitting parameters for equations on thermal conductivity

Equation	Symbol	values	Unit	R^2
5	λ_{r0}	0.69	W/m/K	0.98
	k_e^{λ}	0.30	W/m/K	
	k_{cu}^{λ}	0.15	W/m/K	
	χ_{λ}	0.32	-	
8	β_0	0.78	W/m/K	0.98
	k_e^{β}	0.68	W/m/K	
	χ_{β}	1.44	-	
9	ϑ_0	0.74	-	0.99
	k_{cu}^{ϑ}	13.85	-	
	χ_{ϑ}	2.33	-	

Note: λ_{r0}, k_e^{λ}, k_{cu}^{λ}, χ_{λ}, β_0, k_e^{β}, χ_{β}, ϑ_0, k_{cu}^{ϑ} and χ_{ϑ} are fitting parameters.

Table 4. Test results on $CaCO_3$ content and increment of thermal conductivity of MICP-treated sands

e	N	C_u	C_{ca}	λ_r	$\Delta\lambda$ (W/m/K)
0.5	5	2	0.82	1.51	0.23
		2.8	0.91	1.68	0.33
		4.7	1.15	1.88	0.44
		9.7	1.22	1.90	0.47
	10	2	1.80	1.82	0.38
		2.8	1.86	2.15	0.55
		4.7	2.09	2.36	0.69
		9.7	2.21	2.43	0.76
	15	2	2.81	2.11	0.50
		2.8	2.84	2.57	0.75
		4.7	3.21	2.88	0.95
		9.7	3.52	3.04	1.08
0.6	5	2	0.75	1.43	0.19
		2.8	0.85	1.61	0.28
		4.7	0.93	1.67	0.32
		9.7	1.01	1.71	0.36
	10	2	1.71	1.70	0.30
		2.8	1.80	1.98	0.44
		4.7	1.91	2.09	0.53
		9.7	1.99	2.11	0.57
	15	2	2.73	1.96	0.42
		2.8	2.77	2.37	0.62
		4.7	2.92	2.55	0.74
		9.7	3.15	2.63	0.83
0.7	5	2	0.70	1.41	0.17
		2.8	0.77	1.49	0.21
		4.7	0.82	1.58	0.26
		9.7	0.88	1.62	0.29
	10	2	1.46	1.59	0.24
		2.8	1.58	1.79	0.33
		4.7	1.70	1.90	0.40
		9.7	1.77	1.92	0.43
	15	2	2.42	1.81	0.33

	2.8	2.49	2.13	0.48
	4.7	2.63	2.31	0.58
	9.7	2.72	2.31	0.61

Note: C_{ca} = $CaCO_3$ contents (Unit: %); λ_r = ratio of thermal conductivity of MICP-treated sand to that of untreated sand; and $\Delta\lambda$ = increment of thermal conductivity (Unit: W/m/K).

Table 5. Fitting parameters for Eq. (7) on increment of thermal conductivity of biocemented sands

C_u	e	β	ϑ	R^2
2	0.5	0.27	0.61	0.99
	0.6	0.22		0.99
	0.7	0.19		0.98
2.8	0.5	0.35	0.72	0.99
	0.6	0.30		0.99
	0.7	0.24		0.99
4.7	0.5	0.40	0.74	0.99
	0.6	0.33		0.99
	0.7	0.28		0.98
9.7	0.5	0.42	0.74	0.99
	0.6	0.35		0.99
	0.7	0.29		0.98

Note: β and ϑ are fitting parameters.

Figure Caption List

Fig. 1. Gradation of Fujian sands: (a and b) percentage finer versus logarithm of particle size, and logarithm of percentage finer versus logarithm of particle size (data from Xiao et al. (2018b)); and (c) scanning electron micrograph of samples with different gradations.

Fig. 2. (Color) Preparation of (a) sand specimen and (b) MICP-treated specimen; and (c) thermal conductivity test.

Fig. 3. (a) Variations of thermal conductivity of untreated specimens with C_u and e; and (b) comparisons between simulations and test results on thermal conductivity of untreated specimens.

Fig. 4. Variations of thermal conductivity properties on MICP-treated sand specimens: (a) λ; (b) R_λ; and (c) $\Delta\lambda$.

Fig. 5. Variations of $CaCO_3$ content on MICP-treated sand specimens: (a) N = 5; (b) N = 10; and (c) N = 15.

Fig. 6. Fitting of increment of thermal conductivity on MICP-treated sand specimens with different void ratios: (a) C_u =2.0; (b) C_u =2.8; (c) C_u =4.7; and (d) C_u =9.7.

Fig. 7. (a)Variations of β with C_u and e; (b) fitting of β with C_u and e; and (c) fitting of ϑ with C_u.

Fig. 8. Predictions on increment of thermal conductivity of MICP-treated sand specimens with $CaCO_3$ content and coefficient of uniformity: (a) e = 0.5; (b) e = 0.6; and (c) e = 0.7.

Fig. 9. Predictions on λ of MICP-treated sand specimens: (a) e = 0.5; (b) e = 0.6; and (c) e = 0.7.

Fig. 10. Verifications of empirical prediction on thermal conductivity and its increment of MICP-treated sand specimens: (a and b) data from the current study; (c and d) data from Martinez et

al. (2019); and (e and f) predictions on test results from Martinez et al. (2019) with respect to $CaCO_3$ content and void ratio.

Fig. 11. Effect of saturation on $CaCO_3$ content and thermal conductivity: (a and b) test results; (c) predictions.

Fig. 12. SEM of MICP-treated sand specimens with the void ratio of 0.5 under the treatment cycle of 15: (a and b) C_u = 2; and (c and d) C_u = 9.7.

Fig. 13. SEM of MICP-treated specimens with C_u = 2.8 and N = 15: (a and b) e = 0.5; and (c and d) e = 0.7.

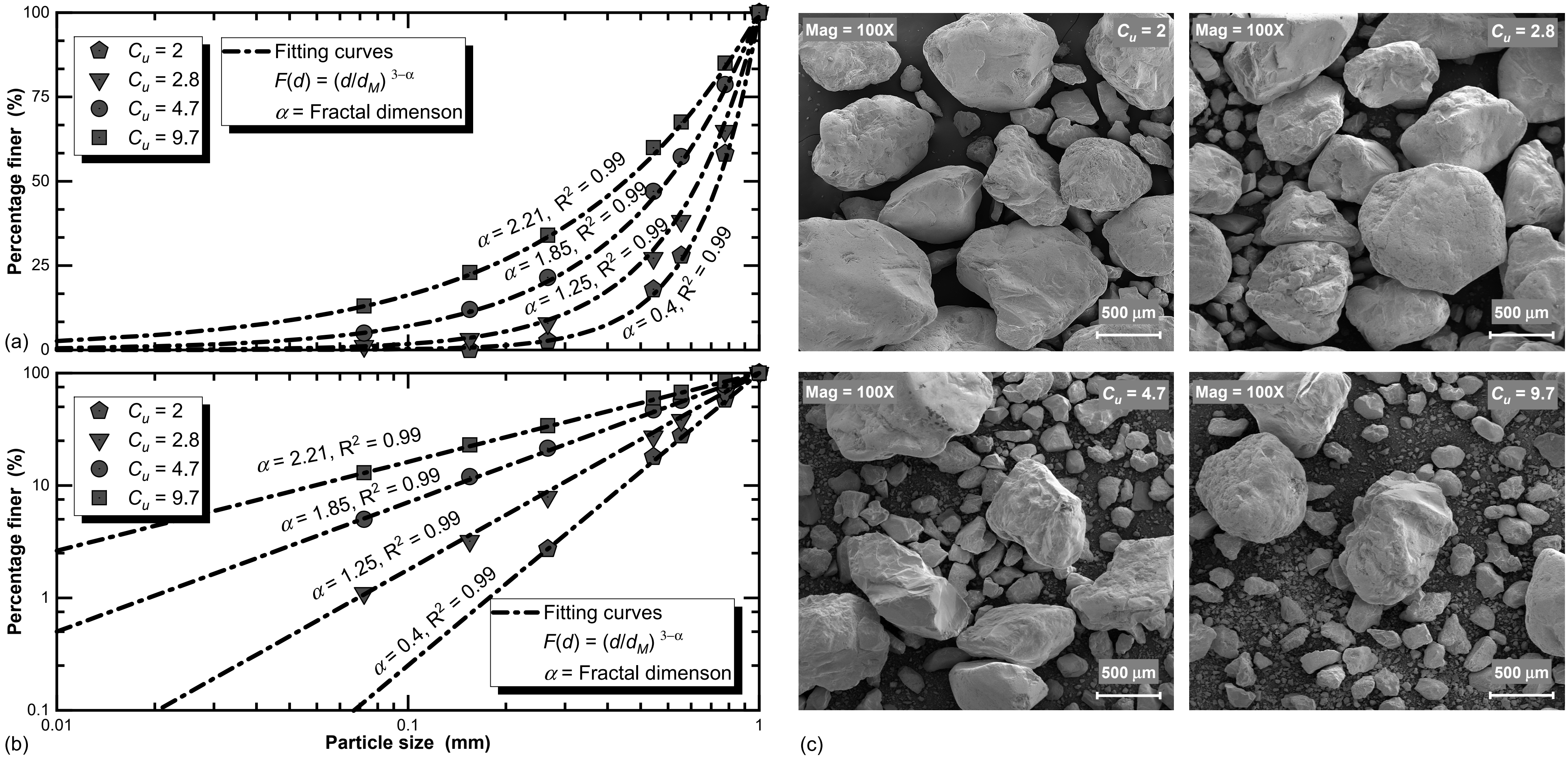

Percentage finer (%)
100
75
50
25
0
C_u = 2
C_u = 2.8
C_u = 4.7
C_u = 9.7
Fitting curves
$F(d) = (d/d_M)^{3-\alpha}$
α = Fractal dimenson
α = 2.21, R^2 = 0.99
α = 1.85, R^2 = 0.99
α = 1.25, R^2 = 0.99
α = 0.4, R^2 = 0.99
(a)
100
10
1
0.1
0.01
0.1
1
Particle size (mm)
(b)
Mag = 100X
C_u = 2
C_u = 2.8
C_u = 4.7
C_u = 9.7
500 µm
(c)

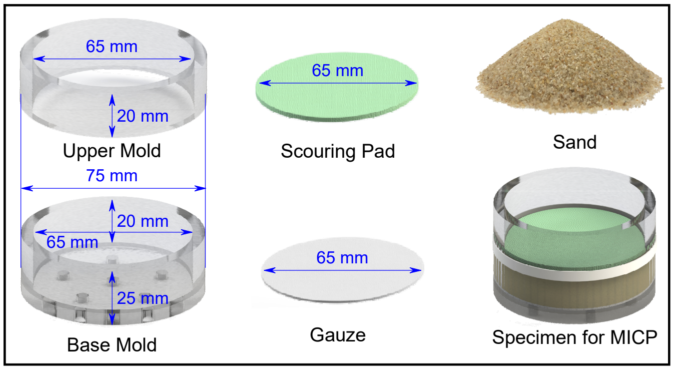
65 mm
20 mm
Upper Mold
75 mm
20 mm
65 mm
25 mm
Base Mold
65 mm
Scouring Pad
65 mm
Gauze
Sand
Specimen for MICP

(a)

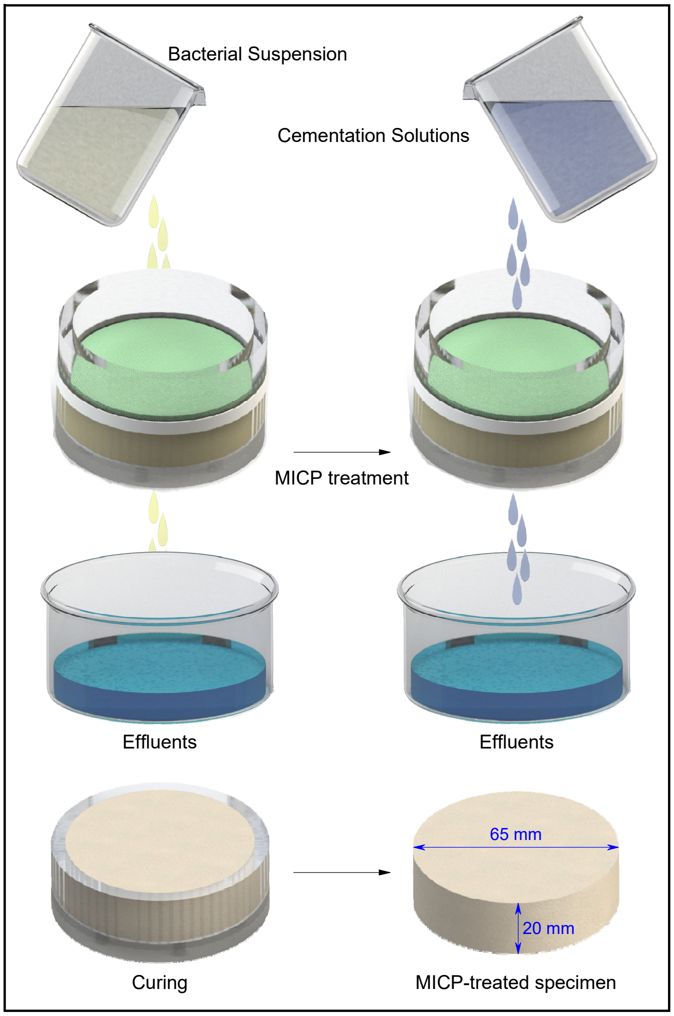
Bacterial Suspension
Cementation Solutions
MICP treatment
Effluents
Effluents
Curing
65 mm
20 mm
MICP-treated specimen

(b)

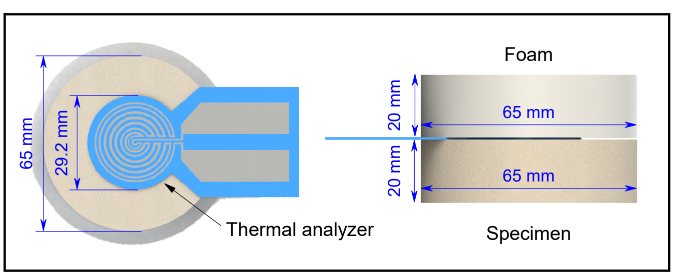
65 mm
29.2 mm
Thermal analyzer
Foam
20 mm
65 mm
20 mm
65 mm
Specimen

(c)

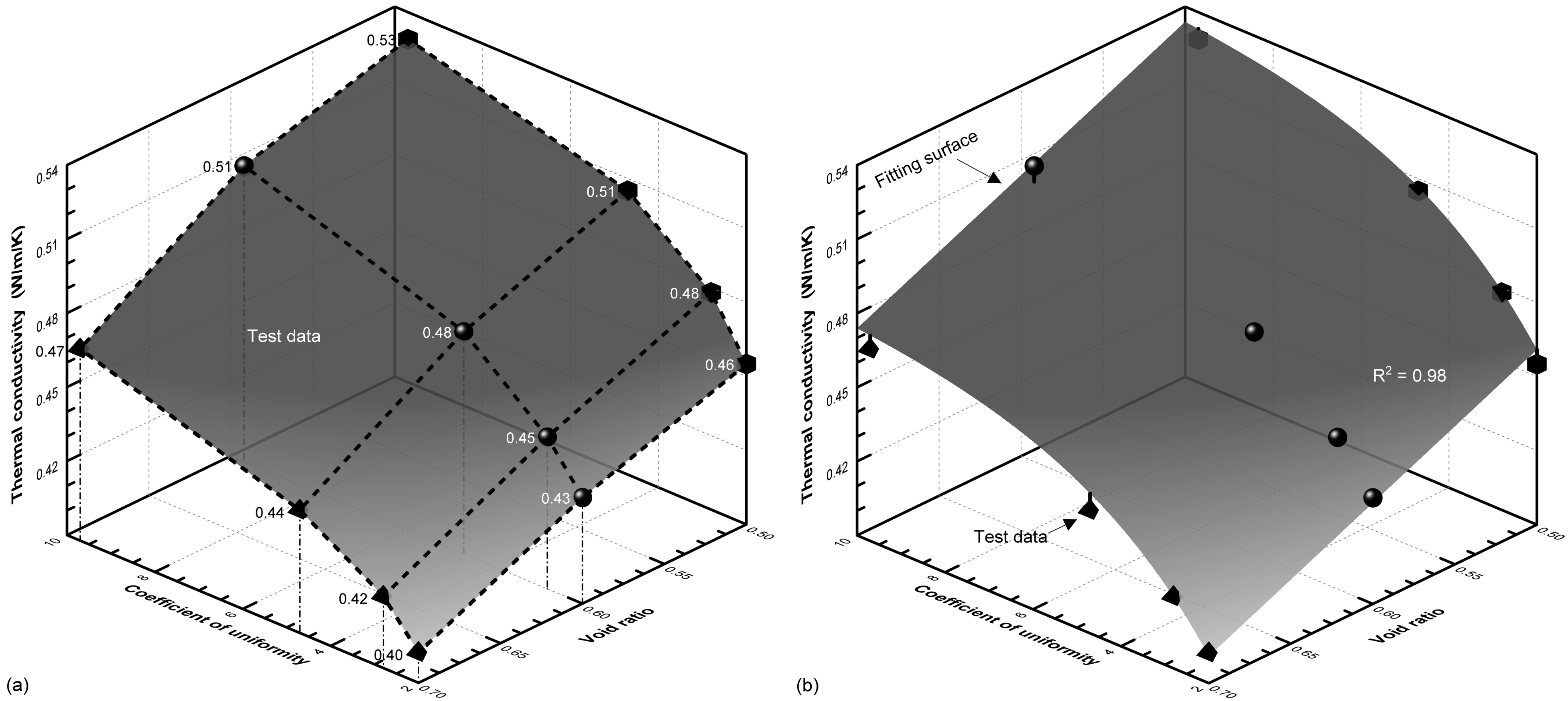
Thermal conductivity (W/mK)
0.54
0.51
0.48
0.47
0.45
0.42
Coefficient of uniformity
10
8
6
4
2
Void ratio
0.50
0.55
0.60
0.65
0.70
0.53
0.51
0.51
0.48
0.48
0.46
0.45
0.44
0.43
0.42
0.40
Test data
(a)
Fitting surface
Test data
R^2 = 0.98
(b)

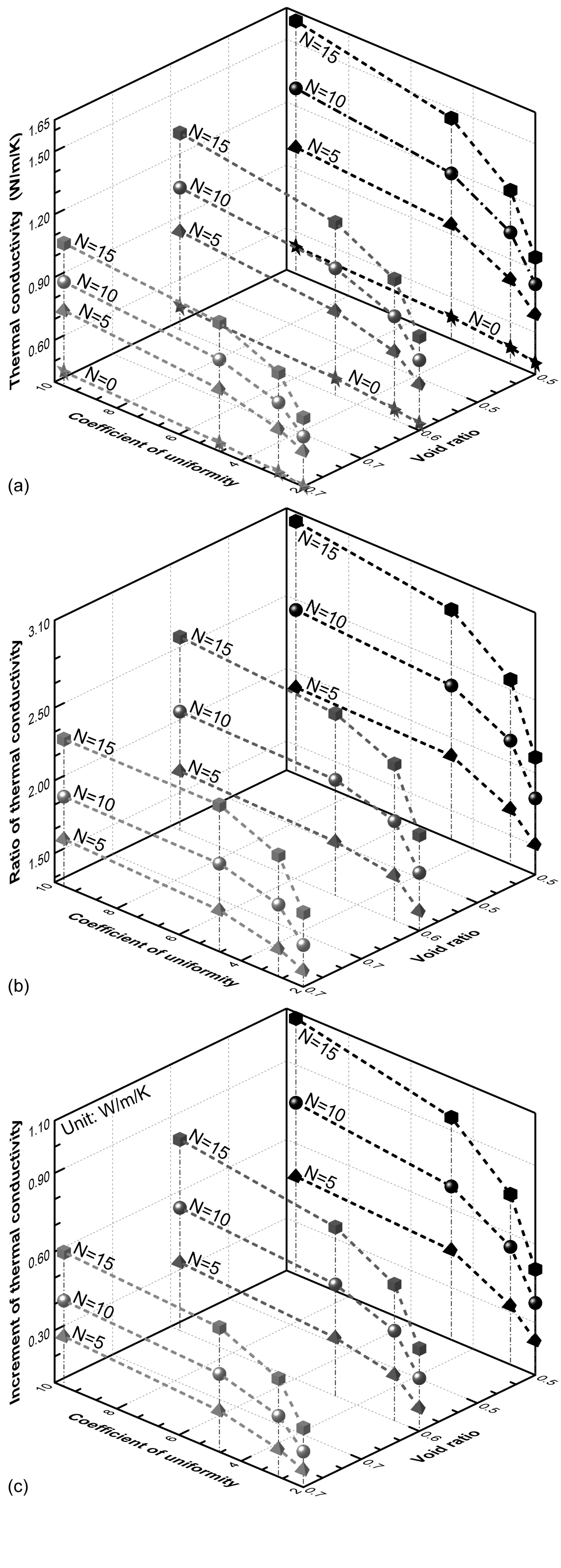

Thermal conductivity (W/m/K)
1.65
1.50
1.20
0.90
0.60
N=15
N=10
N=5
N=0
Coefficient of uniformity
Void ratio
(a)
Ratio of thermal conductivity
3.10
2.50
2.00
1.50
(b)
Increment of thermal conductivity
Unit: W/m/K
1.10
0.90
0.60
0.30
(c)

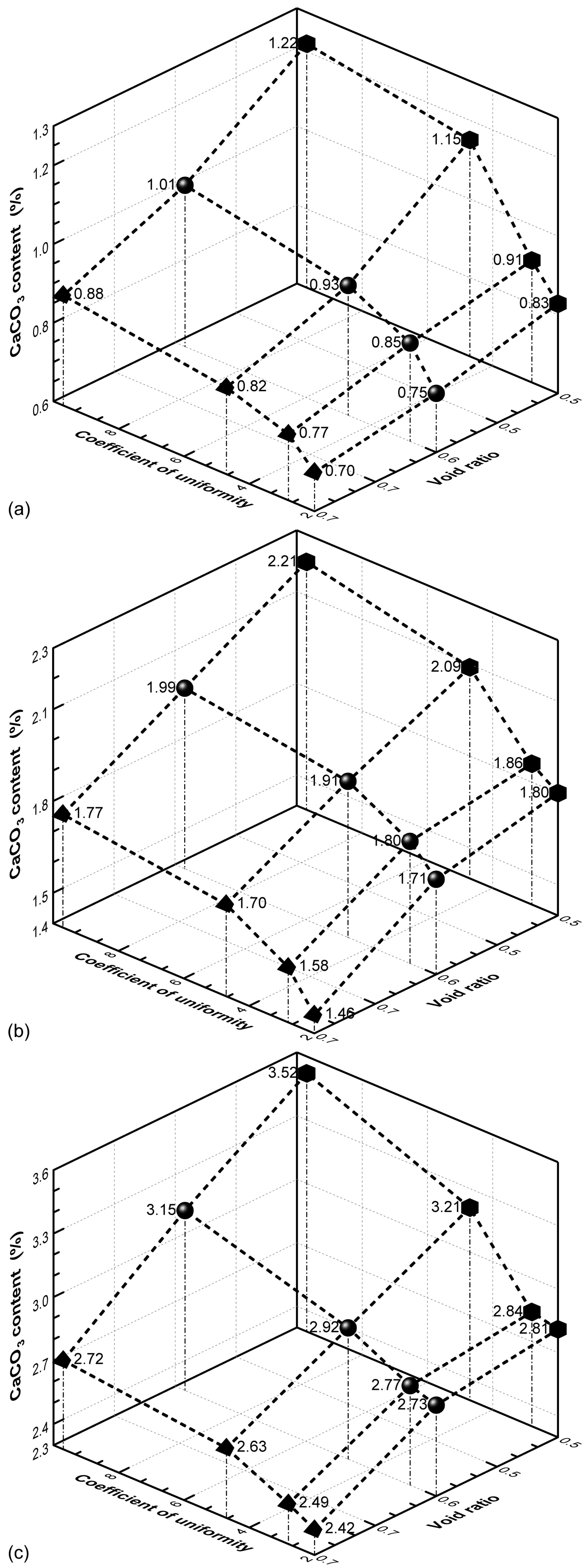
CaCO3 content (%)
Coefficient of uniformity
Void ratio
1.22
1.15
1.01
0.91
0.93
0.83
0.88
0.85
0.75
0.82
0.77
0.70
(a)
2.21
2.09
1.99
1.86
1.91
1.80
1.77
1.80
1.71
1.70
1.58
1.46
(b)
3.52
3.15
3.21
2.84
2.92
2.81
2.72
2.77
2.73
2.63
2.49
2.42
(c)

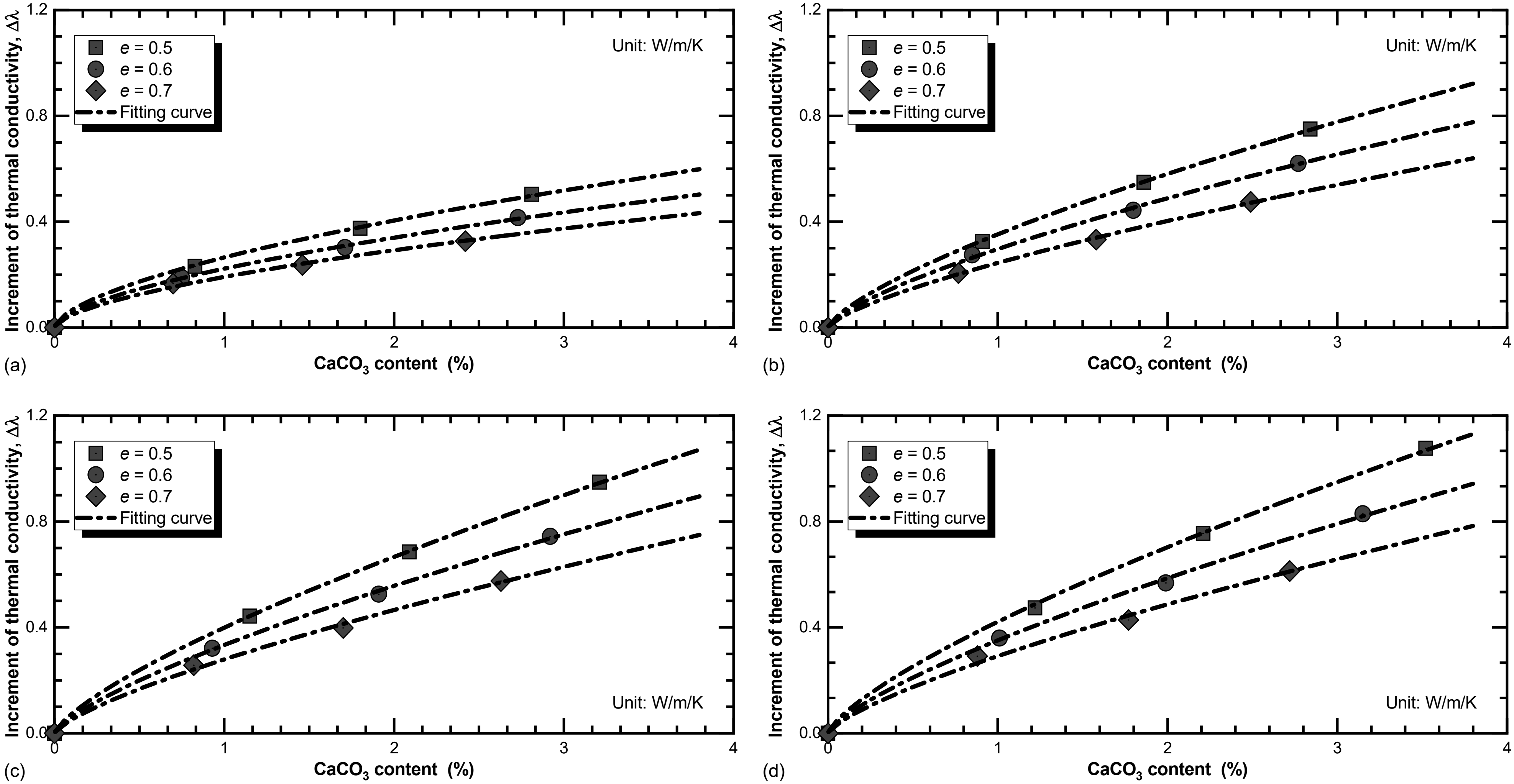

Increment of thermal conductivity, Δλ
CaCO3 content (%)
e = 0.5
e = 0.6
e = 0.7
Fitting curve
Unit: W/m/K
(a)
(b)
(c)
(d)
0.0
0.4
0.8
1.2
0
1
2
3
4

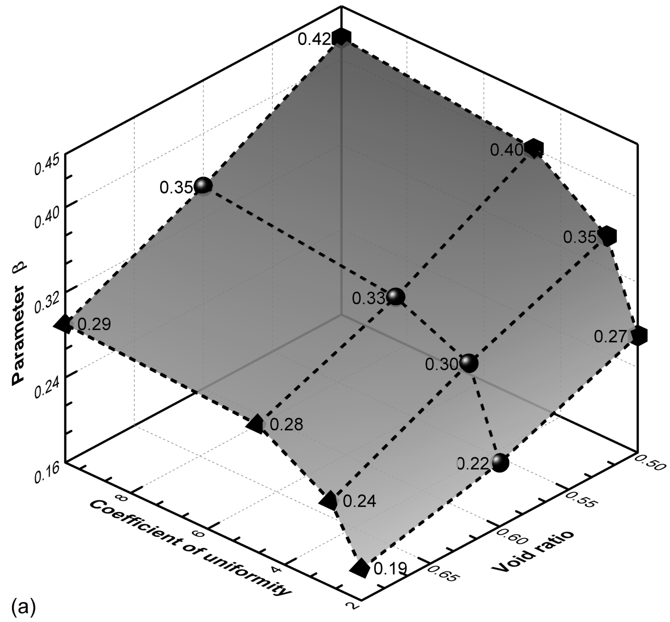

0.42
0.40
0.35
0.35
0.33
0.29
0.27
0.30
0.28
0.22
0.24
0.19
Parameter β
0.45
0.40
0.32
0.24
0.16
Coefficient of uniformity
8
6
4
2
Void ratio
0.50
0.55
0.60
0.65

(a)

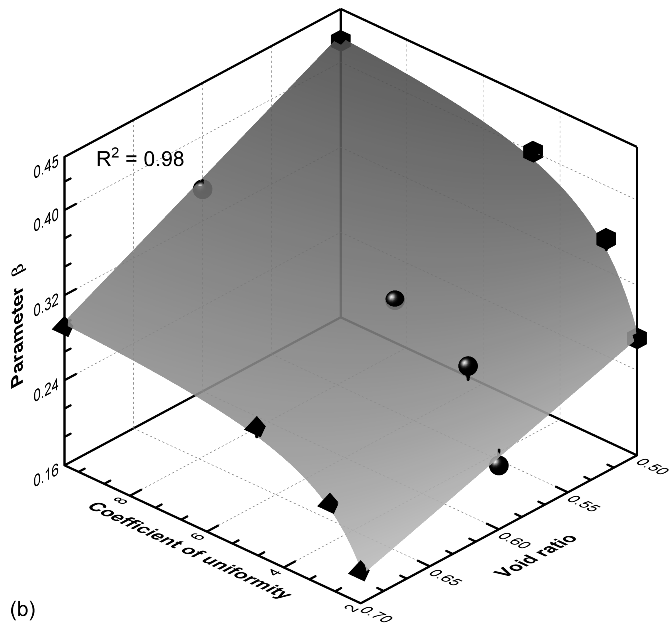

R^2 = 0.98
Parameter β
0.45
0.40
0.32
0.24
0.16
Coefficient of uniformity
8
6
4
2
Void ratio
0.50
0.55
0.60
0.65
0.70

(b)

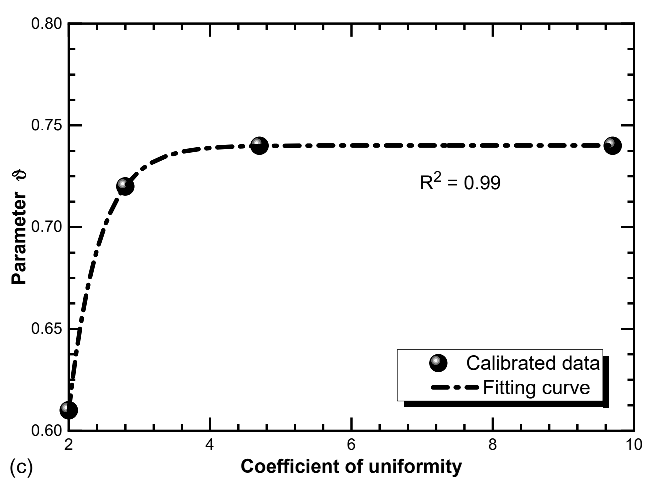

Parameter ϑ
0.80
0.75
0.70
0.65
0.60
R^2 = 0.99
Calibrated data
Fitting curve
2
4
6
8
10
Coefficient of uniformity

(c)

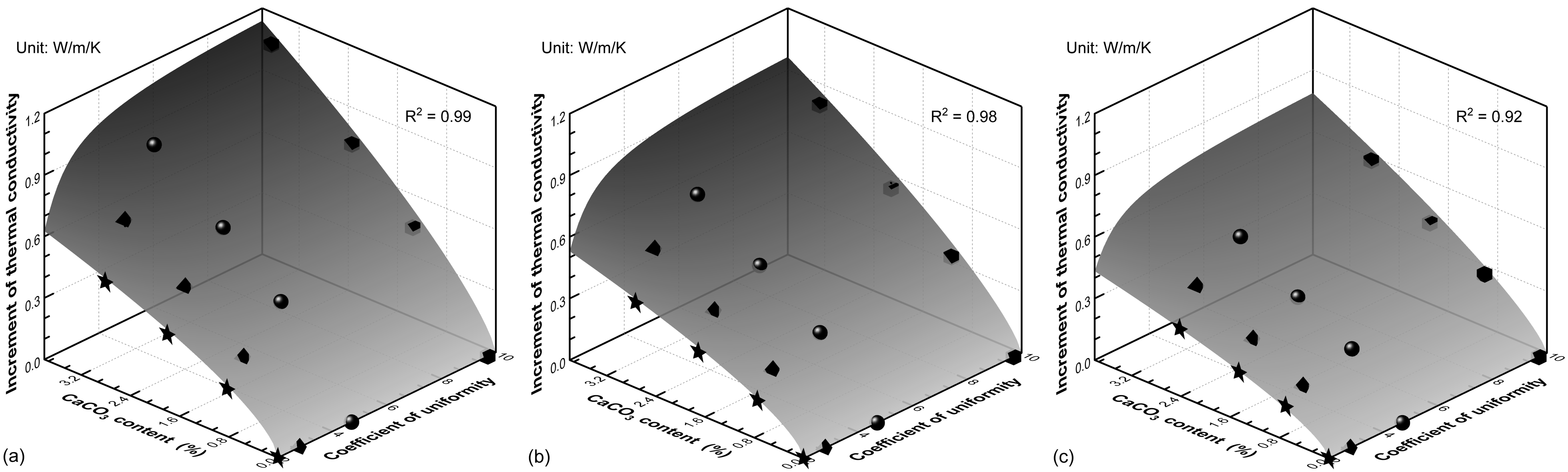
Unit: W/m/K
R^2 = 0.99
Increment of thermal conductivity
$CaCO_3$ content (%)
Coefficient of uniformity
(a)
Unit: W/m/K
R^2 = 0.98
Increment of thermal conductivity
$CaCO_3$ content (%)
Coefficient of uniformity
(b)
Unit: W/m/K
R^2 = 0.92
Increment of thermal conductivity
$CaCO_3$ content (%)
Coefficient of uniformity
(c)

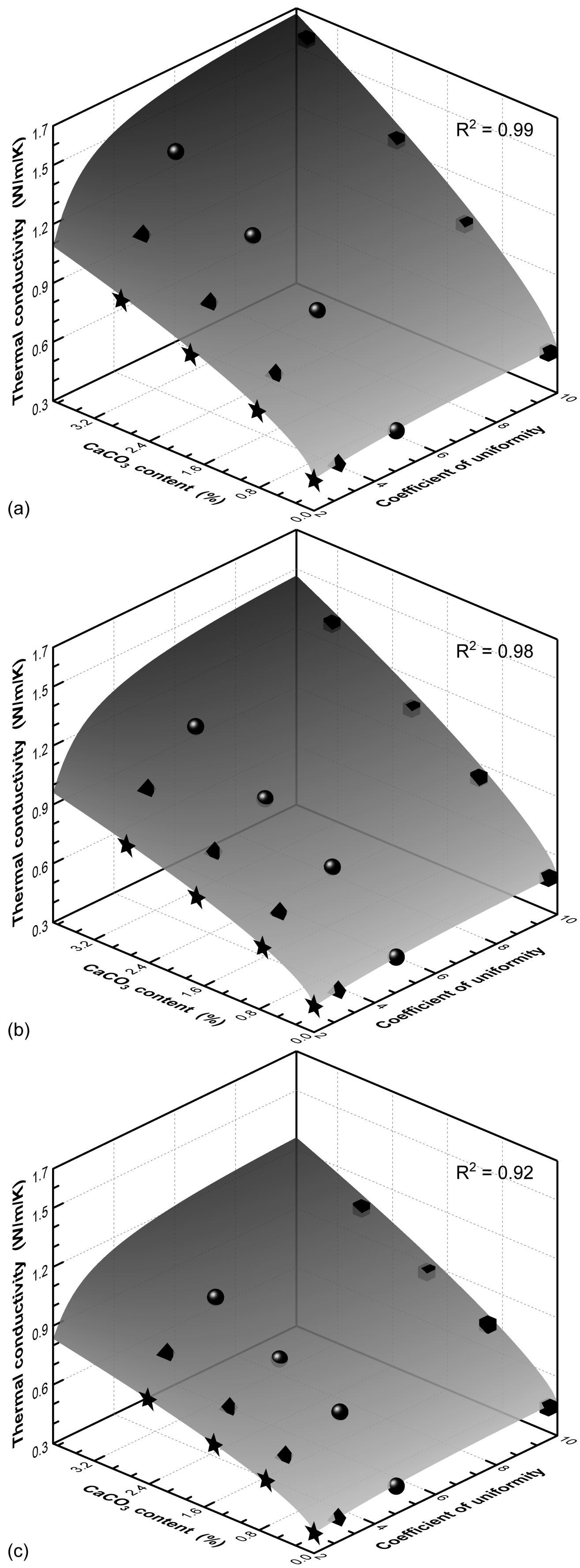
R^2 = 0.99
(a)
R^2 = 0.98
(b)
R^2 = 0.92
(c)
Thermal conductivity (W/mK)
CaCO$_3$ content (%)
Coefficient of uniformity
0.3
0.6
0.9
1.2
1.5
1.7
0.0
0.8
1.6
2.4
3.2
2
4
6
8
10

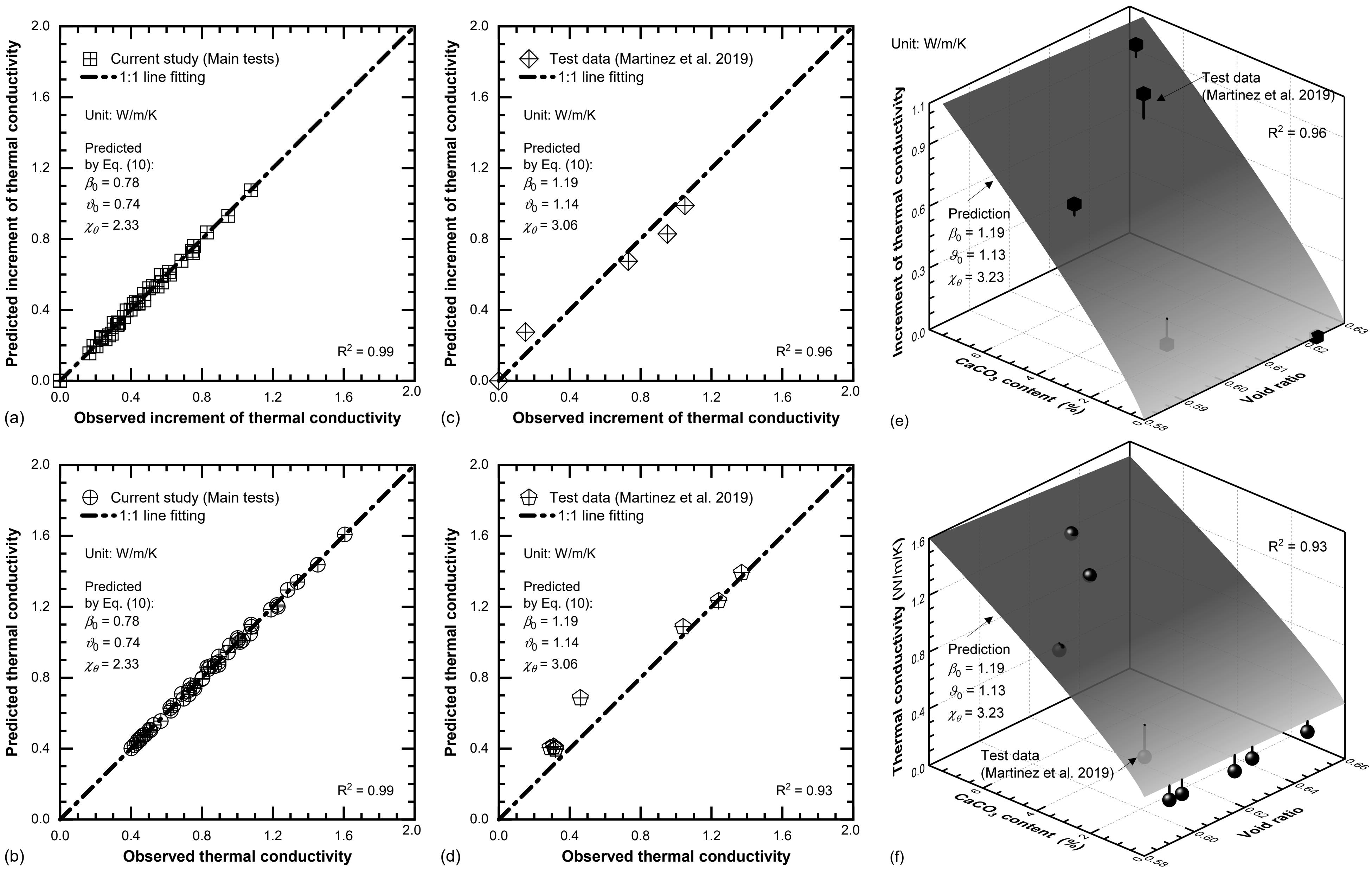

(a)
Current study (Main tests)
1:1 line fitting
Unit: W/m/K
Predicted by Eq. (10):
β_0 = 0.78
ϑ_0 = 0.74
χ_θ = 2.33
R^2 = 0.99
Predicted increment of thermal conductivity
Observed increment of thermal conductivity
(c)
Test data (Martinez et al. 2019)
1:1 line fitting
Unit: W/m/K
Predicted by Eq. (10):
β_0 = 1.19
ϑ_0 = 1.14
χ_θ = 3.06
R^2 = 0.96
Predicted increment of thermal conductivity
Observed increment of thermal conductivity
(e)
Unit: W/m/K
Test data (Martinez et al. 2019)
R^2 = 0.96
Prediction
β_0 = 1.19
ϑ_0 = 1.13
χ_θ = 3.23
Increment of thermal conductivity
$CaCO_3$ content (%)
Void ratio
(b)
Current study (Main tests)
1:1 line fitting
Unit: W/m/K
Predicted by Eq. (10):
β_0 = 0.78
ϑ_0 = 0.74
χ_θ = 2.33
R^2 = 0.99
Predicted thermal conductivity
Observed thermal conductivity
(d)
Test data (Martinez et al. 2019)
1:1 line fitting
Unit: W/m/K
Predicted by Eq. (10):
β_0 = 1.19
ϑ_0 = 1.14
χ_θ = 3.06
R^2 = 0.93
Predicted thermal conductivity
Observed thermal conductivity
(f)
R^2 = 0.93
Prediction
β_0 = 1.19
ϑ_0 = 1.13
χ_θ = 3.23
Test data (Martinez et al. 2019)
Thermal conductivity (W/m/K)
$CaCO_3$ content (%)
Void ratio

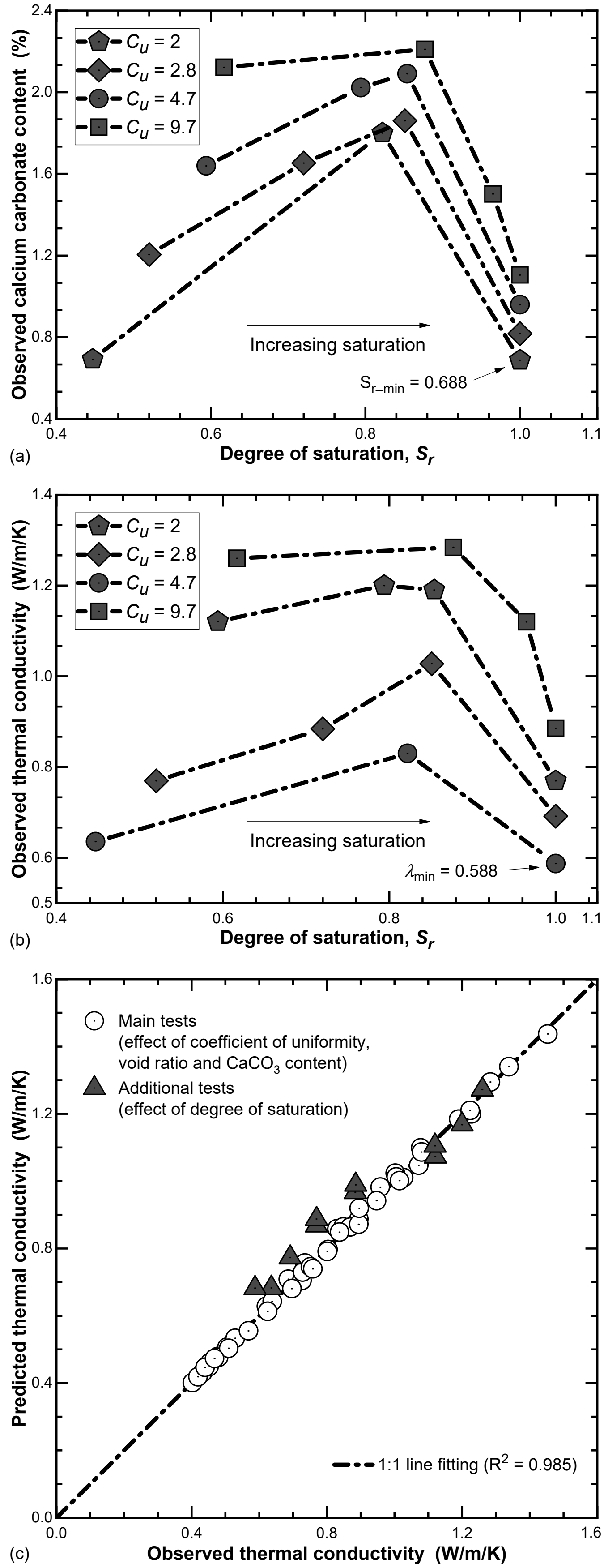

Observed calcium carbonate content (%)
Degree of saturation, S_r
C_u = 2
C_u = 2.8
C_u = 4.7
C_u = 9.7
Increasing saturation
S_{r-min} = 0.688
(a)
Observed thermal conductivity (W/m/K)
Degree of saturation, S_r
Increasing saturation
λ_{min} = 0.588
(b)
Predicted thermal conductivity (W/m/K)
Observed thermal conductivity (W/m/K)
Main tests
(effect of coefficient of uniformity, void ratio and $CaCO_3$ content)
Additional tests
(effect of degree of saturation)
1:1 line fitting (R^2 = 0.985)
(c)

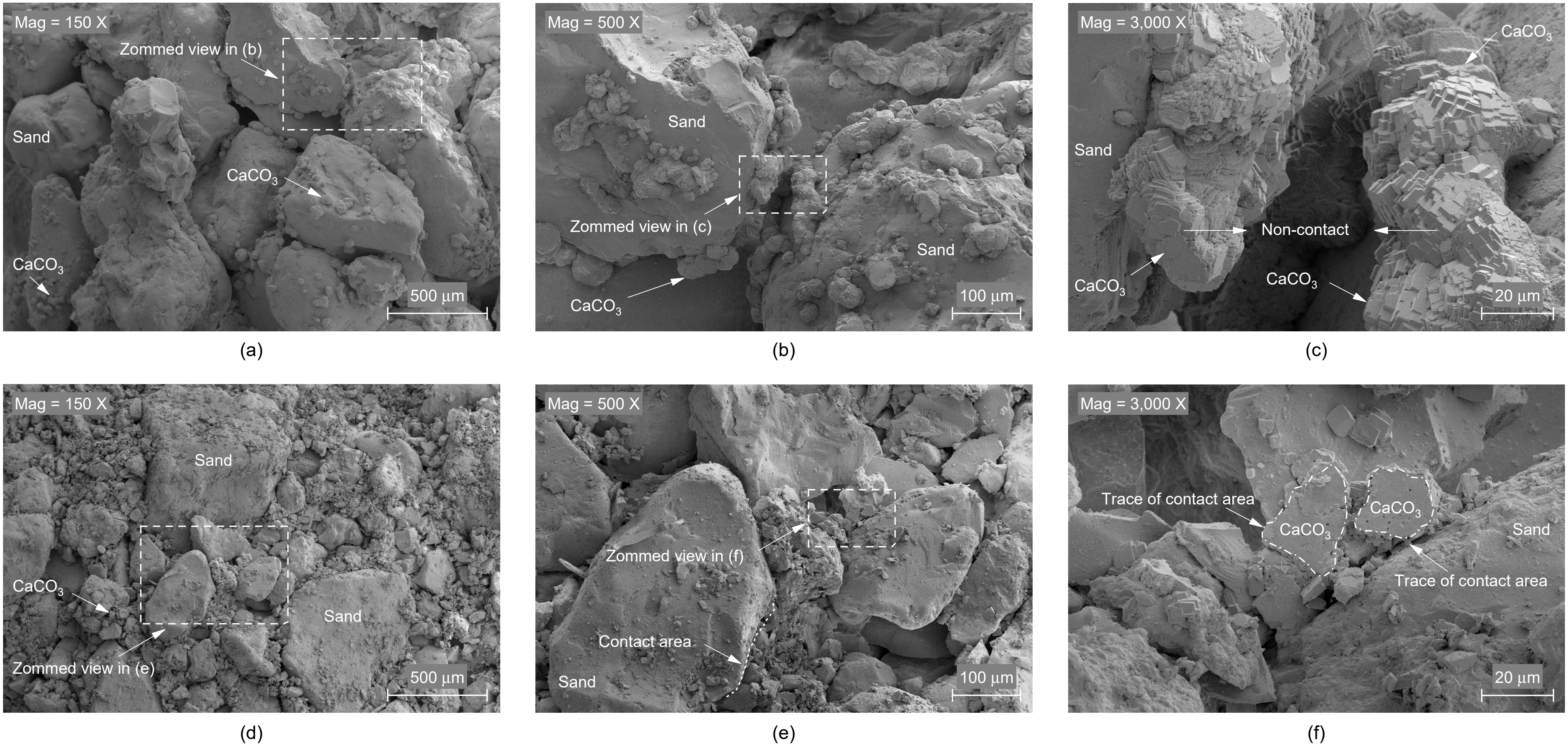
Mag = 150 X
Zommed view in (b)
Sand
$CaCO_3$
$CaCO_3$
500 μm
(a)
Mag = 500 X
Sand
Zommed view in (c)
Sand
$CaCO_3$
100 μm
(b)
Mag = 3,000 X
$CaCO_3$
Sand
Non-contact
$CaCO_3$
$CaCO_3$
20 μm
(c)
Mag = 150 X
Sand
$CaCO_3$
Sand
Zommed view in (e)
500 μm
(d)
Mag = 500 X
Zommed view in (f)
Contact area
Sand
100 μm
(e)
Mag = 3,000 X
Trace of contact area
$CaCO_3$
$CaCO_3$
Sand
Trace of contact area
20 μm
(f)

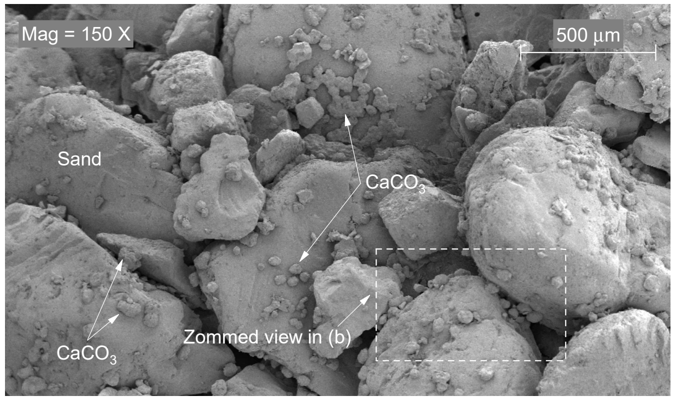
Mag = 150 X
500 μm
Sand
$CaCO_3$
$CaCO_3$
Zommed view in (b)

(a)

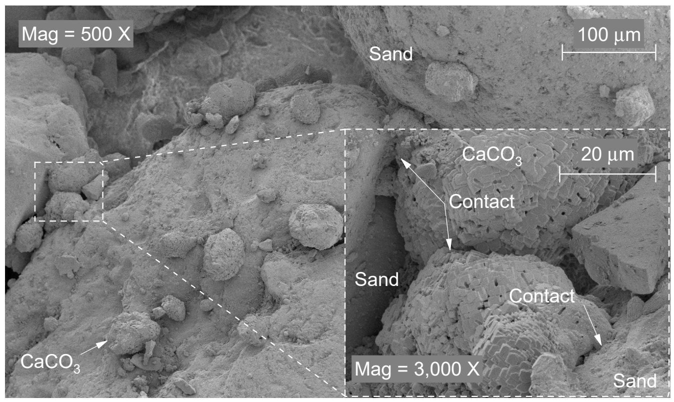
Mag = 500 X
100 μm
Sand
$CaCO_3$
20 μm
Contact
Sand
Contact
$CaCO_3$
Mag = 3,000 X
Sand

(b)

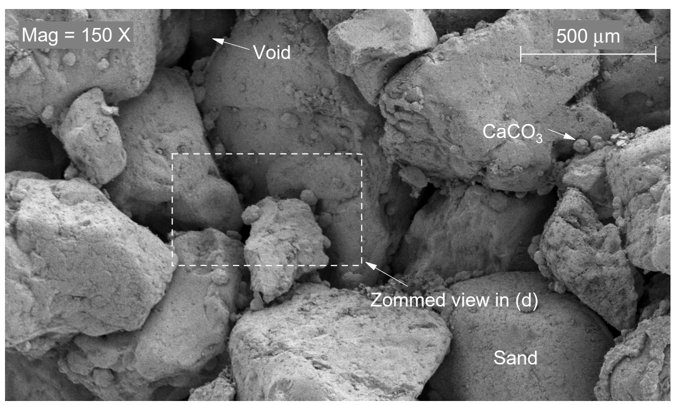
Mag = 150 X
Void
500 μm
$CaCO_3$
Zommed view in (d)
Sand

(c)

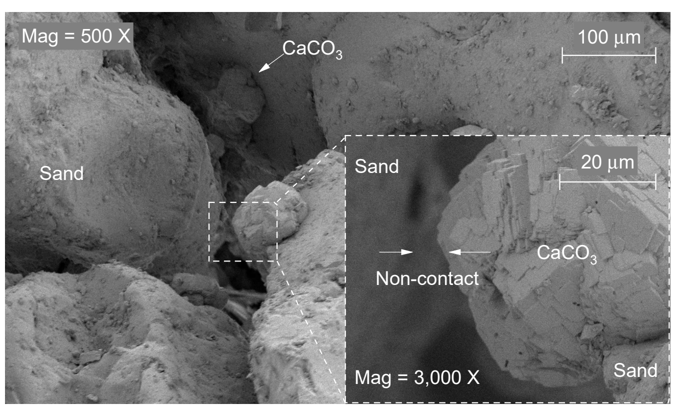
Mag = 500 X
$CaCO_3$
100 μm
Sand
Sand
20 μm
Non-contact
$CaCO_3$
Mag = 3,000 X
Sand

(d)